Fibroblast Growth Factor Receptors Mediate Cellular Senescence in the Cystic Fibrosis Airway Epithelium

*Molly Easter[1], *Meghan June Hirsch[1], Elex Harris[1,2], Patrick Henry Howze IV[1], Emma Lea Matthews[1], Luke I Jones[1], Seth Bollenbecker[1], Shia Vang[1], Daniel J Tyrrell[4], Yan Sanders[3], Susan E Birket[1,2], Jarrod W Barnes[1], Stefanie Krick[1,2*]

[1]Division of Pulmonary, Allergy and Critical Care Medicine, Department of Medicine, The University of Alabama at Birmingham, Birmingham, AL, United States

[2]Gregory Fleming James Cystic Fibrosis Research Centre, The University of Alabama at Birmingham, Birmingham, AL, United States

[3]Eastern Virginia Medical School, Norfolk, VA, United States

[4]Division of Molecular and Cellular Pathology, Department of Pathology, The University of Alabama at Birmingham, Birmingham, AL, United States

*Both authors contributed equally to this manuscript

Corresponding Author: Stefanie Krick MD, PhD

E-mail: skrick@uabmc.edu

Address: McCallum Basic Health Science Building 718, 1918 University Blvd Birmingham, Al USA

Phone number: +1-205- 975-5341

Abstract

The number of adults living with cystic fibrosis (CF) has already increased significantly due to drastic improvements in life expectancy attributable to advances in treatment including the development of highly effective modulator therapy. Chronic airway inflammation in cystic fibrosis (CF) contributes to morbidity and mortality and aging processes like 'inflammaging' and cell senescence impact CF pathology. Our results show that single cell RNA sequencing data, human primary bronchial epithelial cells from non-CF and CF donors, a CF bronchial epithelial cell line, and *Cftr* knockout (*Cftr*$^{-/-}$) rats all demonstrated increased cell senescence markers in the CF bronchial epithelium. This was associated with upregulation of fibroblast growth factor receptors (FGFRs) and mitogen-activated protein kinase (MAPK) p38. Inhibition of FGFRs, specifically FGFR4 and to some extent FGFR1 attenuated cell senescence and improved mucociliary clearance, which was associated with MAPK p38 signaling. Mucociliary dysfunction could also be improved using a combination of senolytics in a CF *ex vivo* model. In summary, FGFR/MAPK p38 signaling contributes to cell senescence in CF airways, which is associated with impaired mucociliary clearance. Therefore, attenuation of cell senescence in the CF airways might be a future therapeutic strategy improving mucociliary dysfunction and lung disease in an aging CF population.

Introduction

Cystic Fibrosis (CF) is the most common autosomal recessive disorder, affecting more than 70,000 people worldwide (1). Respiratory failure is the leading cause of morbidity and mortality in people with CF (pwCF) (2). The emergence of highly effective modulator therapies [HEMT] led to a significant decrease in disease burden and increased life expectancy, but chronic airway inflammation continues to persist thereby affecting many cellular processes leading to accelerated aging and lung function decline (3). Investigations of the aging biology in chronic lung diseases have advanced and several cellular processes, termed "the hallmarks of aging", have been used to characterize and study accelerated aging processes in lung diseases (4). Although, little is known about the aging processes in the CF lung.

Cellular senescence is an aging hallmark defined by irreversible cell cycle growth arrest due to cellular stressors, like inflammation (5). Senescent cells are apoptotic resistant, have increased expression of senescence associated β-gal (SA β-gal), and develop a senescence associated secretory phenotype (SASP) causing tissue damage, inflammation, and paracrine senescence (6). Molecular markers of senescence include B-cell leukaemia/lymphoma 2 (BCL2), B-cell lymphoma-extra-large (BCL-xL) for apoptotic resistance, cyclin-dependent kinase inhibitor 2A (p16), and cyclin-dependent kinase inhibitor 1 (p21) for cell cycle growth arrest, IL-6, IL-8 and IL1-β for SASP and increased expression of SA β-gal (7-9). Cellular senescence contributes to disease pathogenesis and progression in chronic obstructive pulmonary disease (COPD), idiopathic pulmonary fibrosis (IPF) and Alzheimer's Disease. Senolytic drugs targeting senescent cells in these diseases have proven to be beneficial reversing disease course in preclinical models (10).

Fibroblast growth factor receptors (FGFRs) encompass a subfamily of receptor tyrosine kinases that consists of four family members (FGFR1, 2, 3 and 4) with diverse functions (11, 12). FGFR1 and 4

66 are increased in CF and COPD airways and regulate airway inflammation (13, 14). FGFR1 signaling
67 contributes to airway inflammation in CF by activating the extracellular signal-regulated
68 kinase/mitogen-activated protein kinase (ERK-MAPK) signaling cascade (13). FGFR4 induces
69 airway inflammation through phospholipase C γ (PLCγ)/calcineurin and nuclear factor of activated
70 T-cells (NFAT) signaling (13, 14). FGFR signaling plays a complex role in cellular senescence with
71 both pro- and anti-senescence qualities (15-17). However, no studies to date have examined the
72 consequences of cellular senescence and accelerated aging in the CF bronchial epithelium. To our
73 knowledge, this will be the first study to characterize cellular senescence in both *in vitro* and *in vivo*
74 models of CF lung disease. We show that MAPK p38 signaling regulates cellular senescence in the
75 CF bronchial epithelium and seems to involve FGFR4 and partially FGFR1 making FGFR blockade
76 a novel and potential future amenable therapeutic target for senolytic therapies targeting the CF lung,
77 which is independent of CFTR function.

78

79 Results

80 Single-cell RNA sequencing data from primary CF airway epithelial cells demonstrated evidence of
81 cellular senescence

82 To characterize cell senescence in the CF bronchial epithelium in a large, representative CF patient
83 cell cohort, single-cell RNA sequencing (scRNA-seq) data of airway epithelial cells from the
84 previously published GSE150674 dataset was used (18). This dataset includes donors with end stage
85 CF lung disease and healthy controls and ages ranging 6-60 years in CF (n=17,590 cells and n=19
86 donors) and 18-63 years in healthy donors (n=23119 cells and n=19 donors). Using uniform manifold
87 approximation and projections (UMAPs), the dataset contains a variety of cell types (Suppl. Figure
88 1A) with the majority consisting of basal, ciliated and secretory cells in both control and CF donors

(Suppl. Figure 1B). For our analysis, we filtered the CF cell population to cells homozygous for the DF508 mutation (n= 10,131 cells and n=8 donors with age range of 25-60 years) and created 3 senescence signature scores visualized via UMAPs and violin plot from three gene sets: CellAge senescence inducing genes (408 genes) database (19), SenoMayo (124 genes) (20) and a commonly used cellular senescence marker panel (*CDKN1A, CDKN2A, BCL2, BCL2L1, IL6, IL1B and GLB1*). UMAPs and violin plots examining the senescence score from the CellAge database showed a significant increase in the CF cohort compared to controls (Figure 1A, B). Furthermore, the SenoMayo score mean was significantly increased in the CF group compared to controls with noticeable differences in the UMAP between CF and control groups (Figure 1C, D). Moreover, we created a cellular senescence score using the following cellular senescence markers: *CDKN1A, CDKN2A, BCL2, BCL2L1, IL6, IL1B and GLB1,* which demonstrated significant differences in the combined score visually and via violin plot in the CF epithelial cell group compared to control (Figure 1E, F).

In order to identify the specific cell types involved, we subclassified the airway epithelial cells into the major representing groups and found significant differences in cellular senescence scores based on cell type. Using the CellAge database senescence score, basal and secretory epithelial cells from CF donors had a significantly increased score, when compared to non-CF controls, whereas there was no difference between ciliated cells from CF and control donors (Figure 1G). Similar results were seen using the SenoMayo score (ciliated CF cells showed a decrease in senescence markers) (Figure 1G) and the 8 gene senescence score (Figure 1G). Overall, these data support the evidence of cellular senescence in the CF airway epithelium using multiple senescence scores with large datasets of genes associated with cellular senescence, which seems to be primarily localized to basal and secretory airway cells.

Single-cell RNA sequencing data revealed an increase in cell senescence in CF airway epithelial cells homozygous for the DF508 mutation.

To further characterize cellular senescence in GSE150674, we filtered the dataset to compare senescence scores in homozygous ΔF508, CF airway cells harboring other CF mutations, and control cells. Senescence scores in ΔF508 CF airway cells and Non-D508 CF airway cells were increased as shown via UMAPs, when compared to control (Suppl. Figure 2A-C). Violin plots comparing the three groups showed a marked increase in all three senescence scores just in the ΔF508 CF airway cells (Suppl. Figure 2D). Overall, these data suggest that the CF airway cells from donors homozygous for the ΔF508 mutation exhibit increased senescence markers.

Primary human bronchial epithelial cells from CF donors expressed increased cellular senescence markers

To validate the findings from the RNAseq dataset, primary human bronchial epithelial cells, cultured at the air liquid interface (ALI) from CF donors, homozygous for the ΔF508 mutation, and non-CF controls were assessed for the expression of an established set of cell senescence markers (7). Similarly, to the cells from the RNAseq dataset, the differentiated primary CF ALI cultures also mainly consisted of basal cells, which were a higher percentage in non-CF donors (70%) versus CF donors (53%) with similar abundance of ciliated cells (18% non-CF vs 22% CF) and more secretory cells in the CF donor lungs, compared to the non-CF controls (25% vs 11%) (Suppl. Figure 3A, B). Using western blot imaging and densitometric analysis, we observed increases in p16, p21 and BCL-xL protein levels in the CF ALI cultures (Figure 2A). SA β-gal staining was increased in CF ΔF508 ALI cultures, when compared to non-CF controls (Figure 2B). Additionally, mRNA levels of the senescence associated secretory phenotype (SASP) (*IL1B ,IL6*, *IL8*) were also substantially increased

in the CF ALI cultures (Figure 2C). Since we have previously shown an association between FGFR signaling and IL-8 secretion in the CF epithelium, including upregulation of FGFR1 (13), we compared the FGF receptor expression between control and CF ALI cultures. Interestingly, most FGFRs were markedly increased in CF ΔF508 primary human bronchial epithelial cells compared to non-CF control ALI cultures (Figure 2D). In summary, markers of cellular senescence and FGFR expression were increased in CF ΔF508 primary human bronchial epithelial cell ALI cultures, when compared to non-CF controls.

To further characterize cell type specific localization of cell senescence markers, we co-labeled ALI cultures with commonly used cell type specific markers and senescence markers which showed that secretory cells, which express uteroglobin (21), also showed expression of p16, p21 and BCL-xL (Suppl. Figure 4A and Suppl. Figure 9B). Co-labeling of basal cells with KRT5 (22), exhibited less co-localization with p16, but overlapped with p21 and BCL-xl as well (Suppl. Figure 4B and Suppl. Figure 9B).

Furthermore, we attempted to validate these findings in human CF lung tissue sections and achieved labeling of secretory cells in sections of the bronchial epithelium, which co-labeled with p16 (Suppl. Figure 5).

FGFR inhibition decreased cellular senescence markers and phosphorylation of p38 MAPK

CF bronchial epithelial cells (CFBEs) were treated with different FGFR inhibitors, including the clinically used FGFR1-3 inhibitor AZD4547 (13, 23-25) and the FGFR4 inhibitor BLU9931 (26). Expression of p16, p21 and BCL-xL showed a marked attenuation following treatment with each specific inhibitor (Figure 3A). Furthermore, the ratio of SA β-gal positive cells in the CFBEs treated with AZD4547 or BLU9931 were substantially lower compared to vehicle treated cells (Figure 3B).

Next, we examined the activation of the downstream signaling mediators of FGFRs including ERK, PLCγ and p38 MAPK (13, 14, 27-30). CFBEs, treated for 24 hours with AZD4547 or BLU9931, did not show any relevant differences in phosphorylation of PLCy or ERK (Figure 3C). However, there was a marked decrease in p38 MAPK phosphorylation in CFBEs treated with AZD4547 or BLU9931 (Figure 3C). Primary human airway CF ALI cultures exhibited a baseline increase in p38 MAPK phosphorylation compared to non-CF controls (Figure 3D).

BLU9931 is a potent, selective and irreversible FGFR4 inhibitor with over 50-fold selectivity over FGFRs 1-3 (16), whereas the clinically established and used inhibitor AZD4547 has selectivity for FGFR1, 2 and 3 at very similar concentrations. In addition, AZD4547 demonstrates weaker activity against FGFR4, VEFGR2 and p38. To further characterize the isoform specific FGFR responsible for the demonstrated "senolytic" effects, we treated CF ALI cultures with PD173074, a potent and more selective FGFR1 inhibitor (IC50 of 25 nM) at 25 and 50 nM (31, 32).

Targeting FGFRs via siRNA knockdown, specifically in ALI cultures, is challenging and will not block residual kinase activity; therefore, inhibitors have been shown to work best for our *in vitro* studies (13, 14). PD173074-treated CF ALI cultures showed a dose dependent reduction in p16 expression (Suppl. Figure 6A) but no changes in p21 and BCL-xL expression (Suppl. Figure 6B, C).

Assessment of the SASP markers IL-6 and IL-8 via ELISA from basolateral media also demonstrated a decrease in PD173074-treated cells, which was in a dose dependent manner for IL-8 (Suppl. Figure 6D). Interestingly, AZD4547 and BLU9931 treatment did not affect IL-6 and 8 levels in the basolateral media of CF ALI cultures (Suppl. Figure 7A,B). In summary, FGFR inhibition attenuated cellular senescence in the CFBEs, which seems to be mediated by FGFR signaling pointing to partial dependence on FGFR1 and a more comprehensive involvement of FGFR4 *in vitro*.

Inhibition of p38 MAPK decreased cellular senescence markers in CFBEs.

To further investigate whether p38/MAPK mediates cellular senescence in the CF bronchial epithelium, CFBEs were treated with a p38/MAPK inhibitor (SB203580) for 24 hours. A marked decrease in protein expression of p16, p21 and BCL-xL was observed following pharmacological blockade of p38/MAPK (Figure 4A). In addition, the SASP cytokines IL-6 and IL-8 were also attenuated by p38/MAPK inhibition in CFBEs (Figure 4B). These findings were also accompanied by a considerable decrease in the ratio of SA β-gal positive cells in CFBEs treated with the p38 MAPK inhibitor (Figure 4C). Together, these data suggest that multiple cellular senescence markers are regulated by p38 MAPK in the CF bronchial epithelium.

Cellular senescence markers were increased in lung tissue and the airway epithelium of *Cftr*$^{-/-}$ rats compared to littermate controls.

Six-month old *Cftr*$^{-/-}$ rats, a model that exhibits CF-like airway disease (33), were used to validate our findings of increased cellular senescence *in vivo*. Lung tissue from 6-month-old *Cftr* $^{-/-}$ rats and controls were assessed via immunohistochemistry and showed increased staining of p16, p21 and BCL-xL in the bronchial epithelium (Figure 5A), when compared to littermate controls and secondary antibody control only (Suppl. Figure 8A, B). Furthermore, SA- β-gal staining was increased in the *Cftr* $^{-/-}$ rat lungs compared to controls (Figure 5B). mRNA levels for *Cdkn2a* (p16), *Cdkn1a* (p21), *Bcl2l1 (BCL-xL),* and SASP markers (*Il-1b, Il-6*, *Cxcl2*) from total lung tissue were also significantly increased in comparison to *Cftr*$^{+/+}$ lungs (Figure 5C). To show bronchial localization of some of the senescence markers, we used immunofluorescence staining and co-labeled frozen sections of *Cftr*$^{-/-}$ rat lung tissue demonstrating that there is co-localization of p16 with uteroglobin, a secretory cell marker, and KRT5, a basal cell marker, validating our *in vitro* results

(Figure 6A-B) which was also compared to secondary controls (Suppl. Figure 9A). In summary, there is evidence of cellular senescence in the lung and bronchial epithelium from a well-established *in vivo* model exhibiting CF airway disease.

Fibroblast growth factor receptor expression were increased in the *Cftr*$^{-/-}$ rat lung

Formalin-fixed paraffin embedded sections of total lung tissue from 6 month-old *Cftr*$^{-/-}$ rats were stained with Alcian blue–periodic acid–Schiff (AB-PAS) to recapitulate the previously established muco-obstructive phenotype when compared to controls (Figure 7A) (33). Immunohistochemical analysis using an isoform specific antibody against FGFR4 revealed increased staining of the *Cftr*$^{-/-}$ bronchial epithelium, when compared to airways from wild type littermates (Figure 7B). FGFR4 protein expression, determined by Western blot analysis, was also substantially increased in *Cftr*$^{-/-}$ rat lungs when compared to controls (Figure 7C). A dearth of validated antibodies limited our ability to assess protein expression of FGFRs 1-3, but we have previously shown that FGFR protein expression correlated with mRNA levels; therefore, qRT-PCR was performed and confirmed a marked increase in mRNA levels of *Fgfr1, Fgfr2* and *Fgfr4* in *Cftr* $^{-/-}$ rat lung tissue (Figure 7D). Transcript levels of the FGFRs have been shown previously to corroborate with protein expression (14). In summary, cell senescence markers as well as FGFRs are upregulated in the lungs of 6-month-old *Cftr*-$^{-/-}$ rats.

Treatment of *Cftr*$^{-/-}$ rats with the FGFR inhibitor AZD4547 attenuated cell senescence in the lungs and bronchial epithelium, which correlated with marked improvements in mucociliary clearance

To investigate the effects of FGFR inhibition on "reversal" of cellular senescence *in vivo*, *Cftr*$^{-/-}$ rats were treated with AZD4547 via oral gavage daily for a total of 5 days. Pharmacological blockade of FGFRs with AZD4547 led to a decrease in p16 and p21 staining in the bronchial epithelium of *Cftr*$^{-/-}$

rats compared to sham treated *Cftr*$^{-/-}$ rats (Figure 8A). Furthermore, total lung protein expression of p21 and Bcl-xL from AZD4547-treated *Cftr*$^{-/-}$ rats was significantly decreased when compared to sham treated rats (Figure 8B). A reduction in phosphorylation of p38 MAPK expression (Figure 8C) and IL-8 secretion (Figure 8D) was also observed. Tracheae of AZD4547 treated *Cftr*$^{-/-}$ rats were analyzed via μOCT (Figure 8E,F) demonstrating marked improvements in air surface liquid [ASL] depth but no considerable differences in ciliary beat frequency (CBF) or periciliary liquid (PCL) depth, suggesting treatment with AZD4547 did not negatively affect the functional microanatomy of the lung epithelium (Figure 8E,F). Further, there were substantial improvements in mucociliary transport (MCT) in the AZD4547 treated *Cftr*$^{-/-}$ rat trachea when compared to the vehicle treatment (Figure 8F). Overall, these data validate our *in vitro* findings that there is a decrease in cell senescence markers after FGFR inhibition with functional consequences, leading to improved mucociliary clearance without affecting the microanatomy of the CF airway epithelium.

Isoform specific inhibition of FGFR4 in an *ex-vivo Cftr*$^{-/-}$ rat trachea model decreased cellular senescence and partially restored mucociliary clearance

To validate our *in vitro* findings that FGFR4 inhibition attenuated cell senescence and assess functional outcomes, we utilized an *ex vivo Cftr*$^{-/-}$ rat trachea model (34) and treated with BLU9931(0.1 uM for 24h) (Figure 9). BLU9931 treatment decreased p16 and p21 levels shown through immunohistochemistry staining of *ex vivo Cftr*$^{-/-}$ rat tracheae compared to the vehicle and secondary only controls (Figure 9A and Suppl. Figure 8C). In addition, *Cdkn2a* (p16), *Cdkn1a* (p21), *Bcl2,* and *Bcl2l1* (BCL-xL) (Figure 9B) and SASP markers (*Il1b, Il6, Cxcl2* (IL-8)) (Figure 9C) mRNA levels were also decreased in BLU9931-treated *Cftr*$^{-/-}$ rat tracheae, when compared to vehicle treated *Cftr*$^{-/-}$ tracheae. Treatment with BLU993 also led to marked improvements in mucociliary

clearance including restoration of MCT and increased ASL depth as well as improved ciliary beat frequency without changes in PCL depth (Figure 9D, E). In summary, these data imply that isoform specific inhibition of *Fgfr4* in an *ex vivo* CF model led to restoration of mucociliary clearance, which was accompanied by attenuation of several cell senescence markers.

Treatment with Dasatinib and Quercetin decreased cellular senescence and improved mucociliary clearance in the *ex vivo Cftr*$^{-/-}$ rat trachea model

To test whether cellular senescence itself contributes to mucociliary dysfunction, we utilized a widely used combination of senolytic drugs (Dasatinib and Quercetin: D+Q), which have been shown to attenuate cell senescence in other cell types including the lung (35, 36) and treated *Cftr*$^{-/-}$ rat tracheae with D+Q for 24 hours. As shown previously by others in other systems, D+Q treatment caused a reduction in of p16 and p21 compared to vehicle and secondary only controls (Figure 10A and Suppl. Figure 8C). μOCT assessment of both trachea groups showed that D+Q treatment also led to restoration of mucociliary transport and ASL depth without affecting ciliary beat frequency and PCL depth (Figure 10B,C). Furthermore, *Il1b, Il-6, Cxcl2* mRNA levels were also substantially decreased in D+Q treated *Cftr*$^{-/-}$ tracheae, when compared to vehicle-treated *Cftr*$^{-/-}$ tracheae (Figure 10D). Along with *Cdkn2a* (p16), *Cdkn1a* (p21), and *Bcl2* mRNA levels which were also significantly down regulated with D+Q treatment (Figure 10E). In summary, targeting senescence in the CF airway *ex vivo* using senolytic therapy improves mucociliary clearance.

HEMT did not substantially decrease cellular senescence markers in CF airways

To investigate whether highly effective modulator therapy [HEMT] could affect cellular senescence, we treated CF primary human bronchial epithelial cells on ALI with VX-661/VX-445/VX-770 [ETI]

and vehicle. First, we demonstrated ETI corrected *CFTR* dysfunction by µOCT analysis of ASL depth in CF primary bronchial epithelial cells showing ASL depth restoration (Figure 11A). However, we did not find any difference in protein expression of the cellular senescence markers p16, p21, and BCL-xL (Figure 11B). To further define the effect of ETI on cellular senescence we examined relative expression of SASPs markers and found that there was no difference in relative expression between treated and vehicle-treated groups either (Figure 11C). Additionally, we did not see differences in *CDKN2a* (p16), *CDKN1a* (p21), or *BCL2* with ETI (Suppl. Figure 10A-C) nor did the addition of ETI + FGFR inhibition improve these markers (Suppl. Figure 10A-F). FGFR expression was also not different between groups (Suppl. Figure 11A). Moreover, we assessed cellular senescence in a hG551D rat model, which is receptive to ivacaftor (VX-770) treatment (37). Immunoblots from hG551D rat lungs treated with VX-770 demonstrated no considerable changes in protein levels of the cellular senescence markers p21 and Bcl-xL (Figure 11D) or SASPs markers (Figure 11E). There was also no difference noted in expression of the different *Fgfr* isoforms (Suppl. Figure 11B). Furthermore, the hG551D rat model itself did not exhibit any increase in cell senescence in its lung, when compared to wild type littermates (Suppl. Figure 12A-E). Taken together, these results show that CFTR correction in CF did not attenuate cellular senescence in our *in vitro* and *in vivo* models.

Discussion

In this study, to our knowledge, we seem to be the first to demonstrate evidence of increased cellular senescence in both *in vitro* and *in vivo* CF models, which was paralleled by an increase in FGFR expression. Pharmacological inhibition of FGFRs led to a decrease in cell senescence, which seemed to be at least partially mediated by MAPK p38. The direct role of the FGFR-MAPK p38 signaling

297 axis on cell senescence was also validated in an *in vivo* CF rat model. Furthermore, pharmacological
298 inhibition of the FGFRs altered mucociliary clearance and air surface liquid volume, two important
299 functional outcomes of CF airway disease severity (38). Additionally, using scRNA sequencing data
300 (GSE150674), we were able to validate cellular senescence as a feature of CF airway epithelial cells,
301 (Figure 1), mainly of basal and secretory airway cells, including more comprehensive cell senescence
302 marker panels, which has proven to be useful in studying pathobiology in other lung diseases such as
303 IPF (39).

304 Cellular senescence was first discovered by Hayflick in the 1960s and has since been described as a
305 hallmark of aging and a common feature found in disease and age associated diseases (40). Several
306 studies have shown that removal of senescent cells via senolytic treatments can reduce the number of
307 senescent cells and significantly decrease disease burden in other chronic lung diseases (10, 41). Our
308 study suggests that FGFR inhibition may attenuate expression of several cell senescence markers,
309 which could be transiently expressed in the CF bronchial epithelium or be a sign of dysfunctional
310 repair as it has been shown in the murine alveolar epithelium, when injured (42). Furthermore, our *in*
311 *vitro* data do not point to highly effective CFTR modulator therapy attenuating cell senescence
312 markers in primary ALI homozygous for the D508 mutation, which is also supported by no changes
313 in the hg551D rats, that were treated with Ivacaftor (Fig. 11 and suppl. Fig. 10-12). Nevertheless,
314 those treatments were short term and there might be a benefit in patients, who have been on HEMT
315 long-term, which needs future investigation. In addition, cell senescence markers were predominantly
316 upregulated in the D508 CFBEs, but we did not analyze a sufficient number of G551D donors or
317 donors with nonsense mutations to draw conclusions. Although, hg551D rats did not show increased
318 senescence where cell senescence was observed in $Cftr^{-/-}$ rat airways.

319

FGFR signaling plays a complex role in cellular senescence, and there is evidence for both pro- and anti-senescence effects. For example, FGFR signaling has been shown to induce cellular senescence in pancreatic cancer cells (7, 16); however, FGFRs have been shown to delay or prevent senescence in stem cells, fibroblasts and neurons (15, 17, 43). Additionally, FGFR signaling has been shown to regulate telomerase activity, which prevents telomere shortening and reduces cellular senescence (44).

FGF receptor signaling has been studied extensively by our lab and others in multiple organs including the lung, kidney, heart, and the parathyroid glands (13, 14, 27-30). FGFR1 signaling can occur via binding to FGF23 and α-klotho, leading to activation of ERK. FGFR4 has been shown to be abundantly expressed in the lung and the bronchial epithelium and shows activation and downstream signaling via PLCγ phosphorylation in the COPD lung (14). In our study, all FGFRs were expressed in the bronchial epithelium, which mainly consisted of basal epithelial cells and secretory cells. Those cell types also showed consistent expression of cell senescence markers, which were increased in the CF donors. Interestingly, the RNAseq dataset also showed upregulation of FGFRs in the ΔF508 CF dataset, which was also shown when combined with the senescence scores (Suppl. Figure 13, 14) but there was relatively low expression of FGFR4, which was abundantly expressed and upregulated in the CF ALI cultures and PLCγ phosphorylation was not increased in CFBEs (Figure 3C). Furthermore, FGFR3 was not consistently upregulated in the CF rat lung (Figure 7D). In previous reports, FGFR3 expression was associated with lung cancer (45), whereas FGFR2 played an important role in alveolar epithelial cell homeostasis and survival following injury (46, 47). A previous study found that FGFR1 plays a role in *Cftr* maturation (36) however, to date there is no data suggesting FGFR regulation of cell senescence in the CF lung.

Our results suggest that FGFR inhibition leads to reduced cell senescence markers, which seems to be partially mediated by MAPK p38. Given that cellular senescence is defined by various markers

and involves intricate crosstalk of signaling pathways, FGF receptor signaling may overlap with upstream/downstream signaling molecules causing FGFR compensatory mechanisms (48-50). In addition, tools to target isoform specific FGFRs are limited with FGFR1 knockout mice not being viable and siRNA mediated FGFR knockdown not efficient due to residual tyrosine kinase activity. Therefore, we used a pharmacological approach against FGFR isoforms that has limitations including potential lack of isoform specificity and off target effects . We have shown previously that α-klotho in the CF airways exhibits an anti-inflammatory action and can attenuate FGF23 and TGF-β-mediated IL-8 secretion (13). However, other studies have shown that FGFR inhibition can regulate downstream mediators without a ligand (51). In order to specify which FGFR isoform mainly contributes to mediation of cell senescence, we used isoform specific FGFR inhibitors, which are partially used in clinical studies. Targeting FGFR1 and FGFR4 as specifically as possible, we could demonstrate that both receptors seem to be involved in the regulation of cell senescence markers, but FGFR4 inhibition showed attenuation of cell senescence in a more comprehensive manner (Figure 9). Interestingly, when using AZD4547, which can not only inhibit FGFR1 but also FGFR2 and 3 and other tyrosine kinases, we saw a greater response when compared to a more specific FGFR1 inhibitor (Figure 3 and Suppl. Figure. 6). Those results show that FGFR signaling is complex and receptor isoforms might be able to compensate for each other, which makes validation of those inhibitors also quite challenging in *in vitro* systems that do express all four FGFRs. In addition, many of the cell senescence markers are target genes of NF-kB signaling, but we neither observed any phosphorylation of p65 *in vivo* and *in vitro* nor did FGFR inhibition affect phosphorylation of p65 (Suppl. Figure 15A-C). Further studies are needed to investigate signaling pathways involved as well as upstream signaling regarding which FGF ligands might contribute. The *Fgfr4* knockout mouse is not lethal, though we have shown that the adult mouse develops airway inflammation along with changes consistent with emphysema, but the murine lung is not a great model to study airway

368 biology, especially cystic fibrosis (27, 52). In addition, FGFR4 inhibition has been studied in cancer
369 though whether FGFR4 is a suitable target in cancer therapy is still controversially discussed (53).
370 Future studies could include neutralizing isoform specific FGFR antibodies to avoid off target
371 effects.

372 Furthermore, whether cell senescence is mediating functional outcomes in the CF bronchial
373 epithelium is of interest and our studies potentially show an indirect link with FGFR inhibition
374 improving mucociliary transport and ASL depth. We have shown previously that TGF-β signaling,
375 which is implicated in aging processes in other lung diseases (54, 55), leads to a decrease in ASL
376 volume and Pirfenidone, a therapy for idiopathic pulmonary fibrosis, can restore ASL volume (56).
377 In this manuscript, we show that senolytic therapy with Dasatanib and Quercetin can improve
378 mucociliary transport in an *ex vivo* CF rat model to further support a potential relation between
379 senescence and mucociliary dysfunction (Figure 10). It is not clear how exactly D+Q achieves the
380 effect in our model system; we did not see changes in cell number in vitro but further studies are
381 needed to define whether this effect could be also mediated via MAPK p38. Cell senescence is one
382 hallmark of aging and several other hallmarks will be worth investigating in future studies including
383 other potential aging related contributing pathomechanisms such as the length-associated
384 transcriptome imbalance (57). There are several additional limitations of our study. Most marked
385 differences were seen in CF donors harboring the D508 mutation and the hg551D rat model did not
386 replicate those findings, but the $Cftr^{-/-}$ rat airways exhibited an increase in our studied cell senescence
387 markers and both *ex vivo* and *in vitro* models showed attenuation with FGFR inhibition pointing to
388 the role of FGFRs but not excluding additional contributing pathways such as inflammation itself or
389 ER stress. Furthermore, mainly basal and secretory cells exhibited the senescent state and our studies
390 assessing mucociliary function were done *ex vivo* and not in the primary cell cultures. Regulation of
391 mucociliary transport is complex and with secretory cells not showing marked senescence features,

we assume that senescence of secretory cells could contribute to the decrease in ASL volume and unfavorable mucus composition impeding on ciliary beat frequency.

Therefore, FGFRs could potentially represent a novel target for senolytic therapies, which are applicable for all people with CF independent of their mutations and may become increasingly relevant in a time of lengthening patient lifespan.

Methods

Animals

Sex as a biological variable:

Our study examined male and female animals, and similar findings are reported for both sexes.

All experiments used male and female SD-*Cftr*^{tm1sage} rats (*Cftr*$^{-/-}$) rats or wild type littermate controls at 6 months old as previously described (33). For experiments involving treatment of *Cftr*$^{-/-}$ rats with AZD4547 (Selleck Chemicals; Houston, TX, USA), we divided *Cftr*$^{-/-}$ rats into two groups (n=8 each): treated with 12.5 mg/kg bodyweight AZD4547 dissolved in DMSO with 1% sodium carboxymethyl cellulose (Selleck Chemicals; Houston, TX, USA) or vehicle once daily for five days. Method of delivery was oral gavage which has been used previously (58). hG551D rats (Envigo) were treated with ivacaftor (VX-770) (Selleck Chemicals; Houston, TX, USA) for 14 days at 30mg/kg/day or 3% methylcellulose vehicle by oral gavage (37).

Ex-vivo Cftr $^{-/-}$ rat trachea culture

Tracheae were isolated from 6-month old *Cftr*$^{-/-}$ rats and carefully explanted to culture cassettes according to methods previously published (34). Those cultures were incubated for 5 days with Pneumacult media and then treated with either BLU9931 (0.1 uM) or a combination of Dasatinib and Quercetin (D+Q) at 100nM and 2uM for 24 hours respectively. After treatment, the tracheae were imaged via μOCT and the epithelial cell layer was removed and used for RNA and protein isolation.

Inhibitors

The following inhibitors were used for *in vitro*, *in vivo* and *ex vivo* experiments: AZD4547 (Selleck Chemicals; Houston, TX, USA), PD173074 (Selleck Chemicals; Houston, TX, USA), BLU9931 (Selleck Chemicals; Houston, TX, USA), SB203580 hydrochloride (Tocris Bioscience; Bristol, UK), a selective inhibitor for p38 MAPK (59), Dasatinib and Quercetin (Selleck Chemicals; Houston, TX, USA).

Cell culture

Both primary human bronchial epithelial cells and CFBEdelta508 (CFBEs) (60) were used for experiments and cultured on Snap well filters or plates in medium consisting of Minimum Essential Media (MEM) with L-glutamine, Phenol Red then supplemented with 10% heat-inactivated fetal bovine serum (Atlas Biologicals; Fort Collins, CO, USA), 1% L-glutamine, 1% penicillin/streptomycin and 0.2% plasmocin. Human bronchial epithelial cells from cystic fibrosis (ΔF508) and non-CF donors were provided by the Cell Culture Core of the UAB Cystic Fibrosis Research Center and cultured and differentiated on air liquid surface interface as previously described (13). Briefly, passages 1-2 of the primary cells were seeded and kept in submerged cultures for about one week to expand to the necessary cell numbers and then splitted on filters and differentiated at the ALI for 4-6 weeks until ciliated cells were observed and mucus was produced in

addition to assessment of transepithelial electrical resistance (TEER) (13, 14, 56). In addition, we assessed proportions of cell types, including ciliated, basal and secretory cells at the time cultures were used for experiments (Suppl. Fig. 2).

HEMT treatment

CF primary human bronchial epithelial cells were cultured at the air liquid interface and treated with Tezacaftor (VX-661), Elexacaftor (VX-445), and Ivacaftor (VX-770) (Selleck Chemicals; Houston, TX, USA) for 72 hours at 3uM,1uM and 3uM respectively. The media with ETI was refreshed every 24 hours.

Western Blot

Protein lysates were collected using 1x radio immunoprecipitation assay (RIPA) buffer with 1x Halt protease and phosphatase inhibitor (Thermo Fisher Scientific, Waltham, MA, USA). Proteins were separated on 4-20% precast Ready Gels (Bio-Rad Hercules, CA, USA) and transferred onto polyvinylidene difluoride (PVDF) membranes (Pierce, Thermo Fisher Scientific, Waltham, MA, USA). Membranes were blocked with either 5% BSA or 5% low-fat milk depending on antibody manufacturer recommendations for 30 mins then incubated overnight with the following primary antibodies: rabbit anti-p21, rabbit anti-BCL-xL, rabbit anti-FGFR4, rabbit total and phospho-anti-ERK1/2, rabbit total and phospho-anti-p38 mitogen-activated protein kinase (MAPK), rabbit total and phospho-anti-PLCγ1 (Cell Signaling Technologies, Danvers, MA, USA), mouse anti-β-actin-peroxidase (Sigma, St. Louis, MO, USA) and rabbit anti-p16 (Proteintech, Rosemont, IL, USA) diluted according to the manufacturer's recommendations. After three washes with TBST, membranes were incubated with goat anti-rabbit peroxidase conjugated (Invitrogen, Carlsbad, CA, USA) at 1:6000 in either 5% low fat milk or 5% BSA depending on primary antibody manufacturer

458 recommendations for one hour. After three washes in TBST, the membranes were imaged by
459 chemiluminescence on a ChemiDoc XRS system (Bio-Rad Hercules, CA, USA) and acquired using
460 Image Lab software (Bio-Rad Hercules, CA, USA). Image J (National Institutes of Health, Bethesda,
461 MD, USA) was used to measure densitometry of positive signals on the membranes.

462

463 RNA Extraction and Quantitative Real-Time PCR

464 Total RNA was extracted from rat lungs, primary human cells and CFBEs as previously described
465 (22, 27). Real- time quantitative PCR was performed with the following TaqMan probes: IL-6
466 Hs00174131, IL1-β Hs01555410, CXCL8 Hs00174103, BCL2L1 Hs00236329_m1 GAPDH
467 (4333764F), FGFR1 Rn01478647, FGFR2 Rn01269940, FGFR3 Rn00584799, FGFR4 Rn01441815,
468 BCL2 Rn99999125, p21 Rn00589996, p16 Rn00580664, IL-8 Rn00586403, IL1-β Rn00580432. IL-
469 6 Rn01410330, BCL2L1 Rn06267811_g1, GAPDH Rn01775763 (Invitrogen, Carlsbad, CA, USA).

470

471 Immunohistochemistry

472 Lungs from control and *Cftr*-/- rats were collected and fixed in 10% neutral buffered formalin for 24
473 hours followed by dehydration in ethanol for 24 hours. The tissue was then embedded in paraffin and
474 cut into 3-5 mm sections and mounted on slides. Lung tissue slides were deparaffinized and stained
475 using rabbit anti-p16, rabbit anti-p21 (Proteintech, Rosemont, IL, USA), anti-rabbit FGFR4 antibody
476 (sc-124; Santa Cruz Biotechnology, Dallas, TX, USA), rabbit anti-BCL-xL (Cell Signaling
477 Technologies, Danvers, MA, USA) and developed using a rabbit specific HRP/DAB detection IHC
478 kit (Abcam Cambridge, UK) then counter stained with haematoxylin. The lung sections were stained
479 with Alcian blue–periodic acid–Schiff and haematoxylin and eosin by UAB Comparative pathology
480 laboratory core.

Immunofluorescence

Epithelial subtype ratios and ALI co-localization: Primary CF and non-CF bronchial epithelial cells were obtained from the UAB Cell Model and Translation Core upon air liquid interface (ALI) differentiation. The media was aspirated and washed with PBS prior to fixation with 4% paraformaldehyde. Staining methods were adapted from the Cell Signaling Immunostaining Protocol. Briefly, after fixation for at least 24 hours, cells were washed with PBS and permeabilized with 0.1% Triton for 15 mins. The specimen was then washed and blocked with 1% bovine serum albumin (BSA) for 60 mins prior to primary incubation overnight with the following antibodies: Krt5 (1:50), Uteroglobin (1:50), FoxJ1 (1:50), p16 (1:100), p21 (1:100). Secondary antibodies were added at 1:2000 (anti-mouse, anti-rat, anti-rabbit) for two hours in the dark. Cells were then stained with NucBlue (Invitrogen, R37606) for 5 minutes and concurrently mounted using Prolong Gold Mounting Media (Invitrogen, P36930) and sealed with coverslips. After mounting, microscope slides were protected from light and stored at 4°C until imaging. Images were obtained on a Nikon Eclipse Ts2 with red, green, and blue cubes at 20x and cells were counted and subsequently analyzed using ImageJ and Excel respectively.

Primary CF bronchial epithelial cells co-labeled with a cell type marker and a senescence marker were imaged using a Zeiss Axio Observer with fluorescent monochrome Hamamatsu ORCA-Flash 4.0 LT camera and software Zen Blue. Images were obtained at 40X magnification with fixed exposure, gain, and signal threshold settings for each target. Signal threshold was based on negative controls stained only the corresponding secondary antibodies. ImageJ 1.54d (61) and Fiji (62) software was used for image processing.

Rat lung tissue staining: Rat lung tissue sections were co-labeled with a cell type marker and a senescence marker were imaged using a Zeiss Axio Observer with fluorescent monochrome Hamamatsu ORCA-Flash 4.0 LT camera and software Zen Blue. Images were obtained at 40X magnification with fixed exposure, gain, and signal threshold settings for each target. Signal threshold was based on negative controls stained only the corresponding secondary antibodies. ImageJ 1.54d (61) and Fiji (62) software was used for image processing.

Human lung tissue staining: Formalin-fixed, paraffin-embedded (FFPE) CF and non-CF human lung tissue sections were obtained from the University of Alabama Tissue Biorepository (UAB-TBR). The IF protocol was adapted from prior IHC staining protocol (63) and the Abcam Immunofluorescence Protocol. Briefly, FFPE sections were melted for 50 minutes in an over set for 60℃. Slides were then de-paraffinized and rehydrated using Clear-Rite 3 (Epredid, 6901) and 100, 95, and 70% ethanol. Antigen retrieval was obtained using antigen unmasking solution (100x, citrate; Vector Labs H3300) in a steamer for 20 minutes. Tissue sections were then rinsed once in PBS and permeabilized for 5 minutes using 0.1% Triton in PBS prior to blocking in 5% BSA. Tissues were then incubated overnight in primary antibodies Krt5 (1:50, Cytokeratin 5, Invitrogen, MA5-15348), Uteroglobin (1:50, anti-hUteroglobin, R&D Systems, MAB4218), or FoxJ1 (1:50, Anti-Hu/Mo FOXJ1, Invitrogen, 14-9965-82) and rabbit p16 (1:200, ProteinTech). After seven five-minute 1 x PBS washes, the tissue sections were incubated for 45 minutes with the respective secondary antibodies (anti-mouse 488, anti-rat 488, anti-rabbit 568)(Invitrogen) at 1:2000. Seven five-minute 1 X PBS washes were completed again and then tissue sections were incubated with diluted NucBlue (2 drops in 1 mL PBS) for 10 minutes before mounting with Prolong Gold Mounting Media and sealed with coverslips. After mounting, microscope slides were protected from light and stored at 4°C until imaging. Imaging was done on a Nikon Eclipse Ts2 at either 10x or 40x to assess co-localization.

Enzyme-Linked Immunosorbent Assay (ELISA)

ELISAs for the quantitative recognition for IL-6 and IL-8 (Invitrogen, Vienna, Austria) were performed using supernatant from CFBEs after treatment with the different inhibitors as outlined before. ELISA for IL-8 (Abcam Cambridge, UK) was performed on protein lysates normalized to 2mg/mL of total protein in each sample from SHAM and AZD treated *Cftr*-/- rats.

Single-cell RNA sequencing data

Publicly available single-cell RNA sequencing dataset GSE150674 that was previously aligned, filtered, normalized and annotated was used to analyze senescence scores using three separate gene sets(18). From the total dataset of 19 controls and 19 CF donors with end-stage lung disease undergoing lung transplantation. For the analysis, we separated the CF group by CF cells that are ΔF508 homozygous (n=10,131 cells and n=8 donors) with a 34–36-year-old average age for the CF group and compared this CF ΔF508 homozygous group to the healthy donor group (n=23119 cells and n=19) with an average age of 46 years for the control group. Both groups include male and female donors. Using BBrowser 3 software (Bio Turning Inc, San Diego, CA, USA) and three different sets of gene list associated with cellular senescence, we created senescence scores visualized via UMAP and violin plots. The gene sets used in the senescence scores were: CellAge senescence genes database which was filtered for genes that induce cellular senescence(19), SenoMayo (20) and cellular senescence markers used in this study : *CDKN1A, CDKN2A, BCL2, BCL2L1, IL6, IL1B and GLB1*. A list of genes used from SenoMayo and CellAge senescence genes database is included as a supplemental table. Violin plots were made by extracting the signature score data from BBrowser3 and analysed in Prism9 (GraphPad, San Diego, CA, USA).

Senescence associated β-galactosidase staining

Cytochemical staining for senescence associated β-galactosidase was performed using a Senescence associated β-galactosidase Staining kit from Cell signaling (Cell Signaling Technologies, Danvers, MA, USA) #9860 following the protocol provided. Rat tissue slides were counterstained with DAPI (Vector Laboratories, Newark CA, USA). To quantify the amount of β-galactosidase staining we captured three images from different regions of the cell culture plates and counted all cells and all of β-galactosidase positive cells from the three images and made a ratio of β-galactosidase positive cells to total cells counted. CFBE experiments were done in triplicates and primary cell cultures included 3 different donors from CF and non-CF.

Micro-optical coherence tomography

Measurements of functional microanatomic parameters in CF primary human bronchial epithelial cells on ALI and ex vivo tracheae were performed using micro-optical coherence tomography (μOCT), a high-resolution microscopic reflectance imaging system as previously described (64).

Statistics

Data were analysed with Prism9 (GraphPad, San Diego, CA, USA) as previously described (27) using unpaired Student's t test or one way ANOVA for a minimum three independent experiments in duplicate. Data is shown with individual values from each experiment ±SEM. Statistical significance was accepted at p-value of less than 0.05.

Study approval

The Institutional Animal Care and Use Committee at the University of Alabama at Birmingham (UAB) approved all animal protocols.

Data availability

All data associated with this manuscript are present in the paper. The single-cell RNA dataset is publicly available data (dataset GSE150674) and cited in this manuscript.

Conflict of interest

The authors have declared that no conflict of interest exists.

Acknowledgements

We thank Dr. Sixto Leal for the use of his Zeiss Axio Observer microscope and Dr. Ashleigh Riegler for her assistance in immunofluorescence imaging and troubleshooting.

Author Contributions

ME, SK, MJH and JB contributed to the concept and/or design of the study. ME, EH, MJH, SB, SB, SV, ELM, LJ and PH contributed to the acquisition of the data and ME, MJH, EH, LJ, PH, YS, DT, JB and SK contributed to the analysis and interpretation. ME, MJH, JB and SK drafted the manuscript. All authors contributed to the article and approved the submitted version.

Support statement

This work was supported by the National Institutes of Health (R01HL160911 to SK and R01HL152246 to JB), as well as the UAB CF Research Translation Core Center – P30DK072482. ME was supported by a pre-doctoral fellowship through the UAB Research and Development Program – ROWE19R0 (CFF) Fellowship.

References

1. Quon BS, and Rowe SM. New and emerging targeted therapies for cystic fibrosis. *Bmj.* 2016;352.
2. Davies P, Drumm M, and Konstan M. Cystic fibrosis: state of the art. *Am J Respir Crit Care Med.* 1996;154:1229-56.
3. Ferrucci L, and Fabbri E. Inflammageing: chronic inflammation in ageing, cardiovascular disease, and frailty. *Nat Rev Cardiol.* 2018;15(9):505-22.
4. Künzi L, Easter M, Hirsch MJ, and Krick S. Cystic Fibrosis Lung Disease in the Aging Population. *Front Pharmacol.* 2021;12:601438.
5. Campisi J, and d'Adda di Fagagna F. Cellular senescence: when bad things happen to good cells. *Nature reviews Molecular cell biology.* 2007;8(9):729-40.
6. Hernandez-Segura A, Nehme J, and Demaria M. Hallmarks of Cellular Senescence. *Trends in Cell Biology.* 2018;28(6):436-53.
7. Muñoz-Espín D, and Serrano M. Cellular senescence: from physiology to pathology. *Nature reviews Molecular cell biology.* 2014;15(7):482-96.
8. Mas-Bargues C, Borrás C, and Viña J. Bcl-xL as a Modulator of Senescence and Aging. *International Journal of Molecular Sciences.* 2021;22(4):1527.
9. Zhu Y, Armstrong JL, Tchkonia T, and Kirkland JL. Cellular senescence and the senescent secretory phenotype in age-related chronic diseases. *Current opinion in clinical nutrition & metabolic care.* 2014;17(4):324-8.
10. Childs BG, Gluscevic M, Baker DJ, Laberge R-M, Marquess D, Dananberg J, et al. Senescent cells: an emerging target for diseases of ageing. *Nature Reviews Drug Discovery.* 2017;16(10):718-35.
11. Eswarakumar V, Lax I, and Schlessinger J. Cellular signaling by fibroblast growth factor receptors. *Cytokine & growth factor reviews.* 2005;16(2):139-49.
12. Jaye M, Schlessinger J, and Dionne CA. Fibroblast growth factor receptor tyrosine kinases: molecular analysis and signal transduction. *Biochimica et Biophysica Acta (BBA)-Molecular Cell Research.* 1992;1135(2):185-99.
13. Krick S, Baumlin N, Aller SP, Aguiar C, Grabner A, Sailland J, et al. Klotho Inhibits Interleukin-8 Secretion from Cystic Fibrosis Airway Epithelia. *Sci Rep.* 2017;7(1):14388.
14. Krick S, Grabner A, Baumlin N, Yanucil C, Helton S, Grosche A, et al. Fibroblast growth factor 23 and Klotho contribute to airway inflammation. *Eur Respir J.* 2018;52(1).
15. Coutu DL, and Galipeau J. Roles of FGF signaling in stem cell self-renewal, senescence and aging. *Aging (Albany NY).* 2011;3(10):920-33.
16. Sasaki N, Gomi F, Yoshimura H, Yamamoto M, Matsuda Y, Michishita M, et al. FGFR4 inhibitor BLU9931 attenuates pancreatic cancer cell proliferation and invasion while inducing senescence: evidence for senolytic therapy potential in pancreatic cancer. *Cancers.* 2020;12(10):2976.
17. Kang D, Jung SH, Lee GH, Lee S, Park HJ, Ko YG, et al. Sulfated syndecan 1 is critical to preventing cellular senescence by modulating fibroblast growth factor receptor endocytosis. *Faseb j.* 2020;34(8):10316-28.

18. Carraro G, Langerman J, Sabri S, Lorenzana Z, Purkayastha A, Zhang G, et al. Transcriptional analysis of cystic fibrosis airways at single-cell resolution reveals altered epithelial cell states and composition. *Nature Medicine.* 2021;27(5):806-14.
19. Tacutu R, Thornton D, Johnson E, Budovsky A, Barardo D, Craig T, et al. Human Ageing Genomic Resources: new and updated databases. *Nucleic Acids Res.* 2018;46(D1):D1083-d90.
20. Saul D, Kosinsky RL, Atkinson EJ, Doolittle ML, Zhang X, LeBrasseur NK, et al. A new gene set identifies senescent cells and predicts senescence-associated pathways across tissues. *Nat Commun.* 2022;13(1):4827.
21. Reynolds SD, Reynolds PR, Pryhuber GS, Finder JD, and Stripp BR. Secretoglobins SCGB3A1 and SCGB3A2 define secretory cell subsets in mouse and human airways. *Am J Respir Crit Care Med.* 2002;166(11):1498-509.
22. Smirnova NF, Schamberger AC, Nayakanti S, Hatz R, Behr J, and Eickelberg O. Detection and quantification of epithelial progenitor cell populations in human healthy and IPF lungs. *Respir Res.* 2016;17(1):83.
23. Saka H, Kitagawa C, Kogure Y, Takahashi Y, Fujikawa K, Sagawa T, et al. Safety, tolerability and pharmacokinetics of the fibroblast growth factor receptor inhibitor AZD4547 in Japanese patients with advanced solid tumours: a Phase I study. *Invest New Drugs.* 2017;35(4):451-62.
24. Chae YK, Hong F, Vaklavas C, Cheng HH, Hammerman P, Mitchell EP, et al. Phase II Study of AZD4547 in Patients With Tumors Harboring Aberrations in the FGFR Pathway: Results From the NCI-MATCH Trial (EAY131) Subprotocol W. *J Clin Oncol.* 2020;38(21):2407-17.
25. Lam WS, Creaney J, Chen FK, Chin WL, Muruganandan S, Arunachalam S, et al. A phase II trial of single oral FGF inhibitor, AZD4547, as second or third line therapy in malignant pleural mesothelioma. *Lung Cancer.* 2020;140:87-92.
26. D'Agosto S, Pezzini F, Veghini L, Delfino P, Fiorini C, Temgue Tane GD, et al. Loss of FGFR4 promotes the malignant phenotype of PDAC. *Oncogene.* 2022;41(38):4371-84.
27. Easter M, Garth J, Harris ES, Shei RJ, Helton ES, Wei Y, et al. Fibroblast Growth Factor Receptor 4 Deficiency Mediates Airway Inflammation in the Adult Healthy Lung? *Front Med (Lausanne).* 2020;7:317.
28. Faul C, Amaral AP, Oskouei B, Hu M-C, Sloan A, Isakova T, et al. FGF23 induces left ventricular hypertrophy. *The Journal of clinical investigation.* 2011;121(11).
29. Grabner A, Amaral AP, Schramm K, Singh S, Sloan A, Yanucil C, et al. Activation of Cardiac Fibroblast Growth Factor Receptor 4 Causes Left Ventricular Hypertrophy. *Cell Metab.* 2015;22(6):1020-32.
30. Singh S, Grabner A, Yanucil C, Schramm K, Czaya B, Krick S, et al. Fibroblast growth factor 23 directly targets hepatocytes to promote inflammation in chronic kidney disease. *Kidney Int.* 2016;90(5):985-96.
31. Tan YY, Zhou HQ, Lin YJ, Yi LT, Chen ZG, Cao QD, et al. FGF2 is overexpressed in asthma and promotes airway inflammation through the FGFR/MAPK/NF-kappaB pathway in airway epithelial cells. *Mil Med Res.* 2022;9(1):7.
32. Skaper SD, Kee WJ, Facci L, Macdonald G, Doherty P, and Walsh FS. The FGFR1 inhibitor PD 173074 selectively and potently antagonizes FGF-2 neurotrophic and neurotropic effects. *J Neurochem.* 2000;75(4):1520-7.
33. Birket SE, Davis JM, Fernandez CM, Tuggle KL, Oden AM, Chu KK, et al. Development of an airway mucus defect in the cystic fibrosis rat. *JCI insight.* 2018;3(1).
34. Harris E, Easter M, Ren J, Krick S, Barnes J, and Rowe SM. An ex vivo rat trachea model reveals abnormal airway physiology and a gland secretion defect in cystic fibrosis. *PLoS One.* 2023;18(10):e0293367.
35. Justice JN, Nambiar AM, Tchkonia T, LeBrasseur NK, Pascual R, Hashmi SK, et al. Senolytics in idiopathic pulmonary fibrosis: Results from a first-in-human, open-label, pilot study. *EBioMedicine.* 2019;40:554-63.
36. Nambiar A, Kellogg D, 3rd, Justice J, Goros M, Gelfond J, Pascual R, et al. Senolytics dasatinib and quercetin in idiopathic pulmonary fibrosis: results of a phase I, single-blind, single-center,

randomized, placebo-controlled pilot trial on feasibility and tolerability. *EBioMedicine.* 2023;90:104481.
37. Birket SE, Davis JM, Fernandez-Petty CM, Henderson AG, Oden AM, Tang L, et al. Ivacaftor Reverses Airway Mucus Abnormalities in a Rat Model Harboring a Humanized G551D-CFTR. *Am J Respir Crit Care Med.* 2020;202(9):1271-82.
38. Mall MA, Mayer-Hamblett N, and Rowe SM. Cystic Fibrosis: Emergence of Highly Effective Targeted Therapeutics and Potential Clinical Implications. *Am J Respir Crit Care Med.* 2020;201(10):1193-208.
39. Reyfman PA, Walter JM, Joshi N, Anekalla KR, McQuattie-Pimentel AC, Chiu S, et al. Single-Cell Transcriptomic Analysis of Human Lung Provides Insights into the Pathobiology of Pulmonary Fibrosis. *American Journal of Respiratory and Critical Care Medicine.* 2019;199(12):1517-36.
40. Hayflick L. The Limited in Vitro Lifetime of Human Diploid Cell Strains. *Exp Cell Res.* 1965;37:614-36.
41. Burton D. Cellular senescence, ageing and disease. *Age.* 2009;31(1):1-9.
42. Riemondy KA, Jansing NL, Jiang P, Redente EF, Gillen AE, Fu R, et al. Single cell RNA sequencing identifies TGFbeta as a key regenerative cue following LPS-induced lung injury. *JCI Insight.* 2019;5(8).
43. Kang W, and Hébert JM. FGF Signaling Is Necessary for Neurogenesis in Young Mice and Sufficient to Reverse Its Decline in Old Mice. *The Journal of Neuroscience.* 2015;35(28):10217-23.
44. Gančarčíková M, Zemanová Z, Březinová J, Berková A, Včelíková S, Šmigová J, et al. The role of telomeres and telomerase complex in haematological neoplasia: the length of telomeres as a marker of carcinogenesis and prognosis of disease. *Prague Medical Report.* 2010;111(2):91-105.
45. Yin Y, Betsuyaku T, Garbow JR, Miao J, Govindan R, and Ornitz DM. Rapid induction of lung adenocarcinoma by fibroblast growth factor 9 signaling through FGF receptor 3. *Cancer Res.* 2013;73(18):5730-41.
46. Dorry SJ, Ansbro BO, Ornitz DM, Mutlu GM, and Guzy RD. FGFR2 Is Required for AEC2 Homeostasis and Survival after Bleomycin-induced Lung Injury. *Am J Respir Cell Mol Biol.* 2020;62(5):608-21.
47. Shimbori C, and El Agha E. Good Things Come in 2s: Type 2 Alveolar Epithelial Cells and Fibroblast Growth Factor Receptor 2. *Am J Respir Cell Mol Biol.* 2020;62(5):543-5.
48. Sørensen V, Zhen Y, Zakrzewska M, Haugsten EM, Wälchli S, Nilsen T, et al. Phosphorylation of fibroblast growth factor (FGF) receptor 1 at Ser777 by p38 mitogen-activated protein kinase regulates translocation of exogenous FGF1 to the cytosol and nucleus. *Mol Cell Biol.* 2008;28(12):4129-41.
49. Miller DL, Ortega S, Bashayan O, Basch R, and Basilico C. Compensation by fibroblast growth factor 1 (FGF1) does not account for the mild phenotypic defects observed in FGF2 null mice. *Molecular and cellular biology.* 2000;20(6):2260-8.
50. Mendoza MC, Er EE, and Blenis J. The Ras-ERK and PI3K-mTOR pathways: cross-talk and compensation. *Trends in Biochemical Sciences.* 2011;36(6):320-8.
51. Strub MD, Gao L, Tan K, and McCray PB. Analysis of multiple gene co-expression networks to discover interactions favoring CFTR biogenesis and ΔF508-CFTR rescue. *BMC Medical Genomics.* 2021;14(1):1-11.
52. van Doorninck JH, French PJ, Verbeek E, Peters RH, Morreau H, Bijman J, et al. A mouse model for the cystic fibrosis delta F508 mutation. *EMBO J.* 1995;14(18):4403-11.
53. Heinzle C, Erdem Z, Paur J, Grasl-Kraupp B, Holzmann K, Grusch M, et al. Is fibroblast growth factor receptor 4 a suitable target of cancer therapy? *Curr Pharm Des.* 2014;20(17):2881-98.
54. Barnes JW, Duncan D, Helton S, Hutcheson S, Kurundkar D, Logsdon NJ, et al. Role of fibroblast growth factor 23 and klotho cross talk in idiopathic pulmonary fibrosis. *Am J Physiol Lung Cell Mol Physiol.* 2019;317(1):L141-L54.
55. Hecker L, Logsdon NJ, Kurundkar D, Kurundkar A, Bernard K, Hock T, et al. Reversal of persistent fibrosis in aging by targeting Nox4-Nrf2 redox imbalance. *Sci Transl Med.* 2014;6(231):231ra47.
56. Manzanares D, Krick S, Baumlin N, Dennis JS, Tyrrell J, Tarran R, et al. Airway Surface Dehydration by Transforming Growth Factor beta (TGF-beta) in Cystic Fibrosis Is Due to Decreased Function of a

Voltage-dependent Potassium Channel and Can Be Rescued by the Drug Pirfenidone. *J Biol Chem.* 2015;290(42):25710-6.
57. Schmauck-Medina T, Molière A, Lautrup S, Zhang J, Chlopicki S, Madsen HB, et al. New hallmarks of ageing: a 2022 Copenhagen ageing meeting summary. *Aging (Albany NY).* 2022;14(16):6829-39.
58. Santorelli S, Fischer DP, Harte MK, Laru J, and Marshall KM. In vivo effects of AZD4547, a novel fibroblast growth factor receptor inhibitor, in a mouse model of endometriosis. *Pharmacology Research & Perspectives.* 2021;9(2):e00759.
59. Paw M, Wnuk D, Nit K, Bobis-Wozowicz S, Szychowski R, Ślusarczyk A, et al. SB203580-A Potent p38 MAPK Inhibitor Reduces the Profibrotic Bronchial Fibroblasts Transition Associated with Asthma. *Int J Mol Sci.* 2021;22(23).
60. Ehrhardt C, Collnot E-M, Baldes C, Becker U, Laue M, Kim K-J, et al. Towards an in vitro model of cystic fibrosis small airway epithelium: characterisation of the human bronchial epithelial cell line CFBE41o. *Cell and Tissue Research.* 2006;323(3):405-15.
61. Schneider CA, Rasband WS, and Eliceiri KW. NIH Image to ImageJ: 25 years of image analysis. *Nat Methods.* 2012;9(7):671-5.
62. Schindelin J, Arganda-Carreras I, Frise E, Kaynig V, Longair M, Pietzsch T, et al. Fiji: an open-source platform for biological-image analysis. *Nat Methods.* 2012;9(7):676-82.
63. Bollenbecker S, Heitman K, Czaya B, Easter M, Hirsch MJ, Vang S, et al. Phosphate induces inflammation and exacerbates injury from cigarette smoke in the bronchial epithelium. *Sci Rep.* 2023;13(1):4898.
64. Liu L, Chu KK, Houser GH, Diephuis BJ, Li Y, Wilsterman EJ, et al. Method for quantitative study of airway functional microanatomy using micro-optical coherence tomography. *PLoS One.* 2013;8(1):e54473.

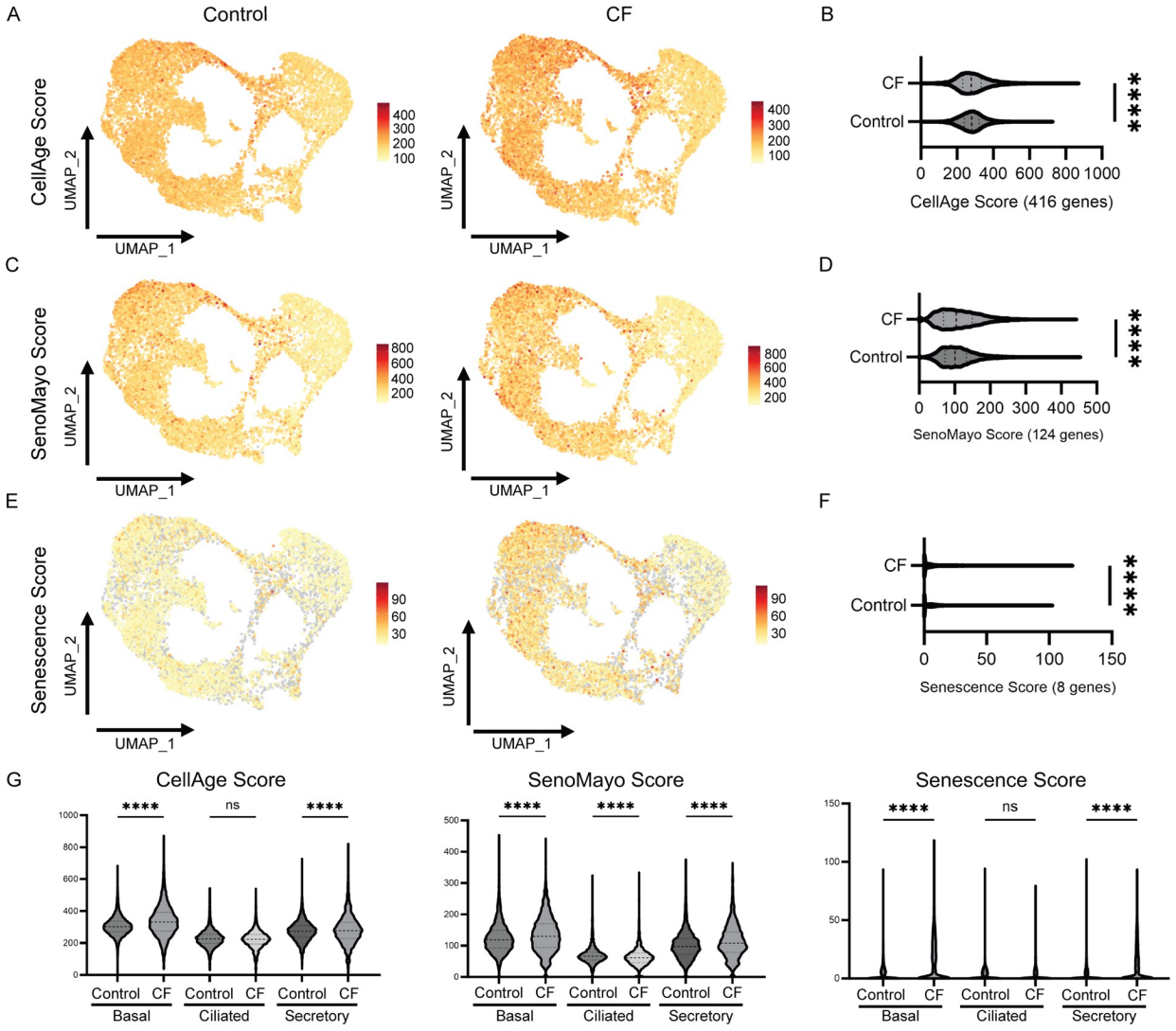

Figure 1: Single-cell RNA sequencing data reveals an increase in cell senescence markers in CF epithelial cells compared to control epithelial cells. Single cell RNA (scRNA) transcriptome of control and CF epithelial cells (GSE150674 Control (CO) and Cystic Fibrosis (CF) epithelial cell count CO n= 23119 and CF n= 17590) from 19 control and 19 CF donor lungs from donors with end stage CF lung disease and healthy controls, CF ΔF508 homozygous patients (n=10,131 cells and n=8 donors) and healthy donors (n=23119 cells and n=19) were separated from the whole dataset and analysed using BBrowser3 to generate UMAPs and violin plots showing senescence scores from three separate gene databases: (A,B) CellAge database of senescence inducing genes (416 genes), (C,D) SenMayo (124 genes), and (E,F) cellular senescence markers used in this study (*CDKN1A, CDKN 2A, BCL2, BCL2L1, IL6, IL1B, IL6 and GLB1*). (G) Senescence scores using the same three gene databases listed above but separated into violin plots looking at senescence scores based on major epithelial cell types: basal, ciliated and secretory. Statistical analysis was done using unpaired Student's t-test or one-way Anova shown with *$p < 0.05$, **$p < 0.01$, ***$p < 0.001$ and **** $p<0.0001$.

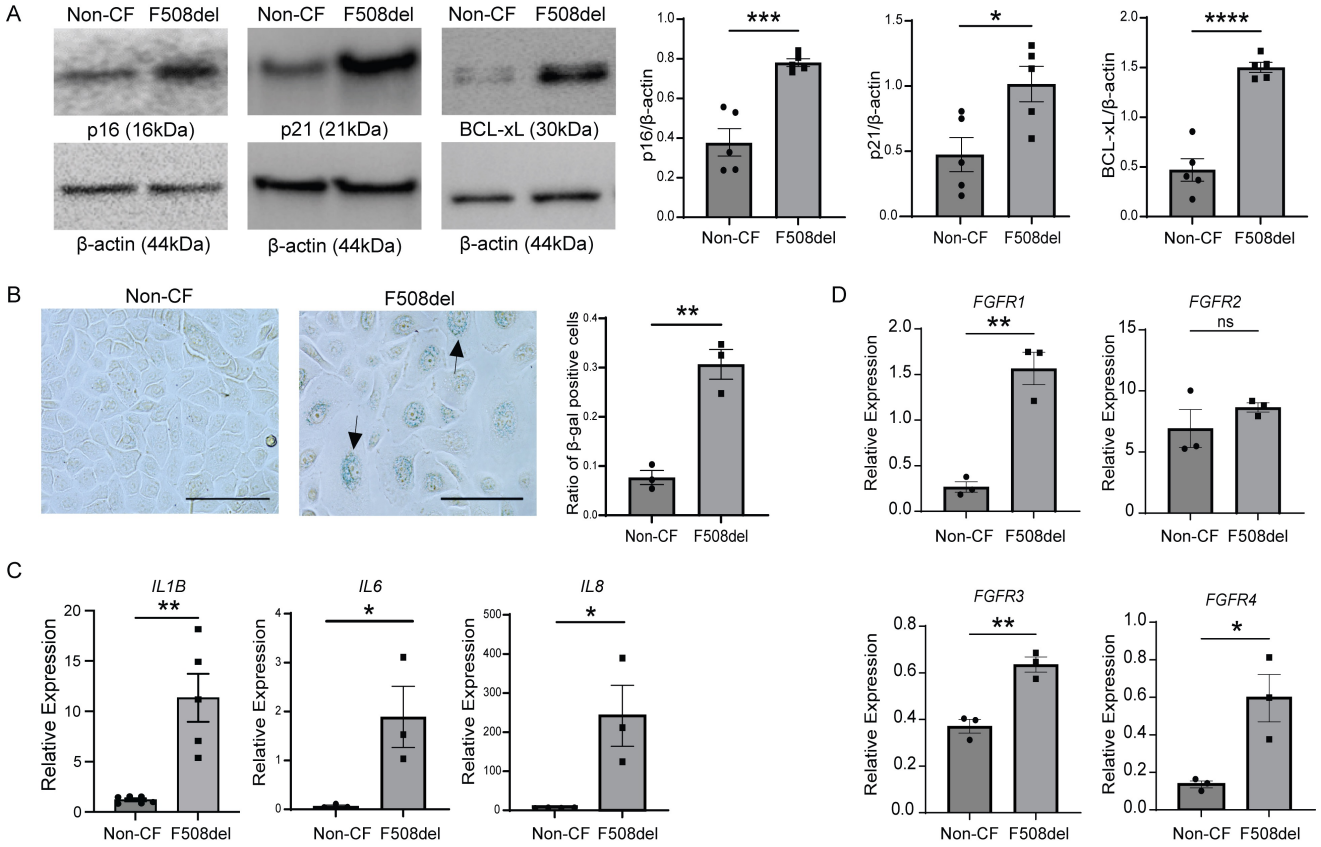

Figure 2: Cellular senescence markers are increased in CF primary human bronchial epithelial cells, cultured at the air liquid interface (ALI). (A) Representative immunoblot images and bar graphs showing densitometric analyses for p16, p21 and BCL-xL in CF ΔF508 and non-CF donors at ALI (N=5). (B) Representative images for senescence associated β-galactosidase (SA-β-gal) staining using brightfield imaging of the same CF ΔF508 and non-CF donor ALI cultures including quantification of β-gal staining using the ratio of SA-β-gal positive cells per brightfield by image J (N=3), arrows show β-gal positive cells (Scale bar = 100uM, Magnification 40x). (C) Bar graphs demonstrating relative mRNA levels of SASPs (*IL1B, IL6, and IL8*) markers normalized to GAPDH. (D) Bar graphs indicating relative mRNA levels of *FGFR1-4* normalized to GAPDH in the same two groups. Statistical analysis was done using unpaired Student's t-test showing means ± SEM with *$p < 0.05$, **$p < 0.01$, and ***$p < 0.001$ from 3-5 different donors per group with experiments repeated 3 times.

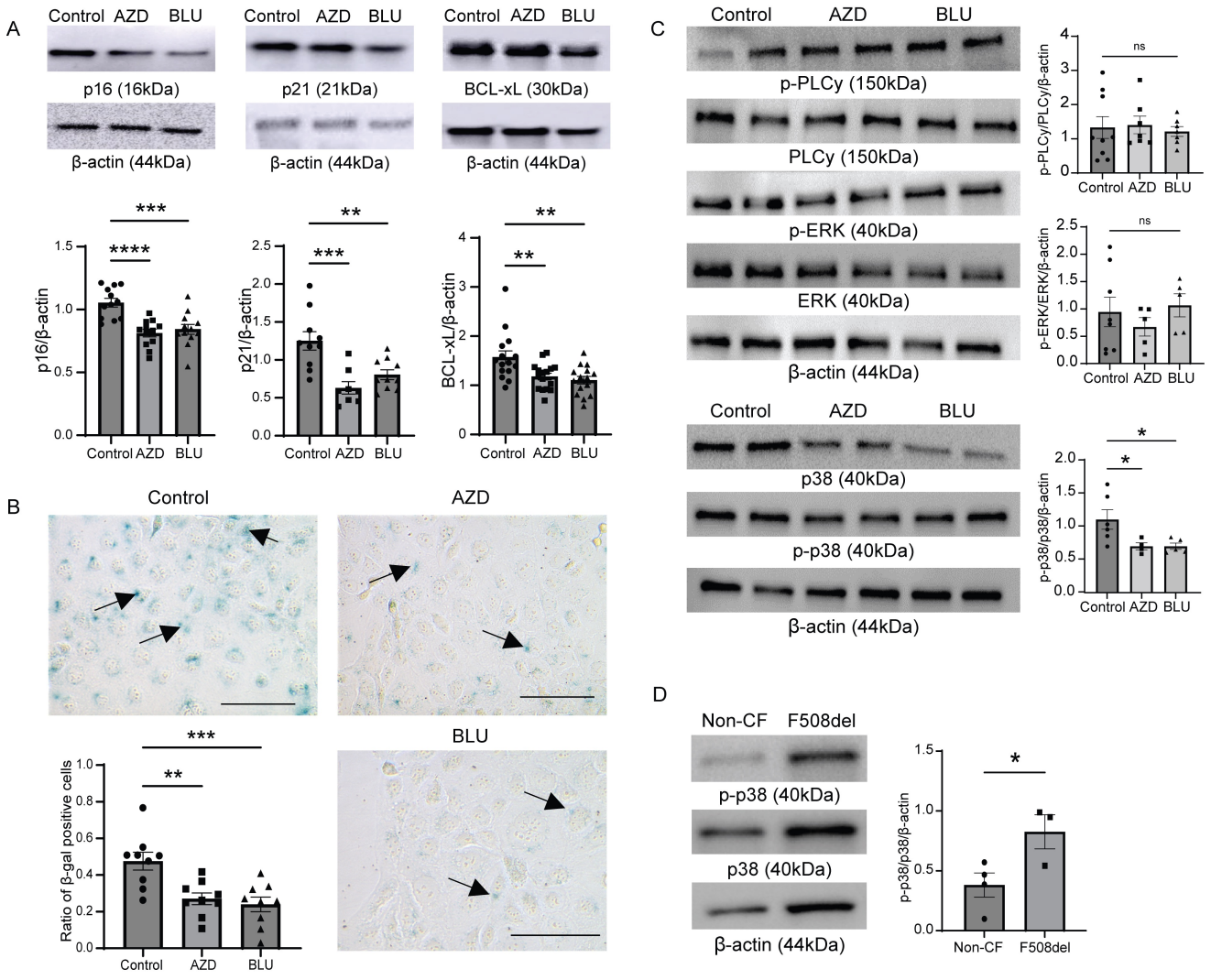

Figure 3: FGFR inhibition decreases cellular senescence markers and decreases phosphorylation of p38 MAPK. (A) Representative immunoblot images and densitometric analyses of the cellular senescence markers p16, p21, and BCL-xL from CFBEs, which were treated with AZD4547 0.1uM or BLU9931 0.1uM for 24 hours. (B) Representative images of SA- β-gal staining's in CFBEs treated with AZD4547 and BLU9931 and quantification by capturing three images from different regions of the cell culture plates and counting total cells and β-gal positive cells from the three images to make a ratio of β-gal positive cells to total cells, arrows indicate β-gal positive cells (scale bar= 100uM, Magnification 40x). (C) Representative immunoblots and densitometric analysis for p-ERK/ERK, p-PLC/PLCγ and p-p38/p38 MAPK in CFBEs treated with AZD4547 and BLU9931 for 24 hours with β-actin loading control (D) Representative immunoblot images and densitometric analyses from primary bronchial epithelial ALI cultures of CF (ΔF508) donors and non-CF control donors for p-p38/p38 MAPK expression. Statistical analysis was done using unpaired Student's t-test showing means ± SEM with *$p < 0.05$, **$p < 0.01$, and ***$p < 0.001$; 3 independent experiments were done in triplicates.

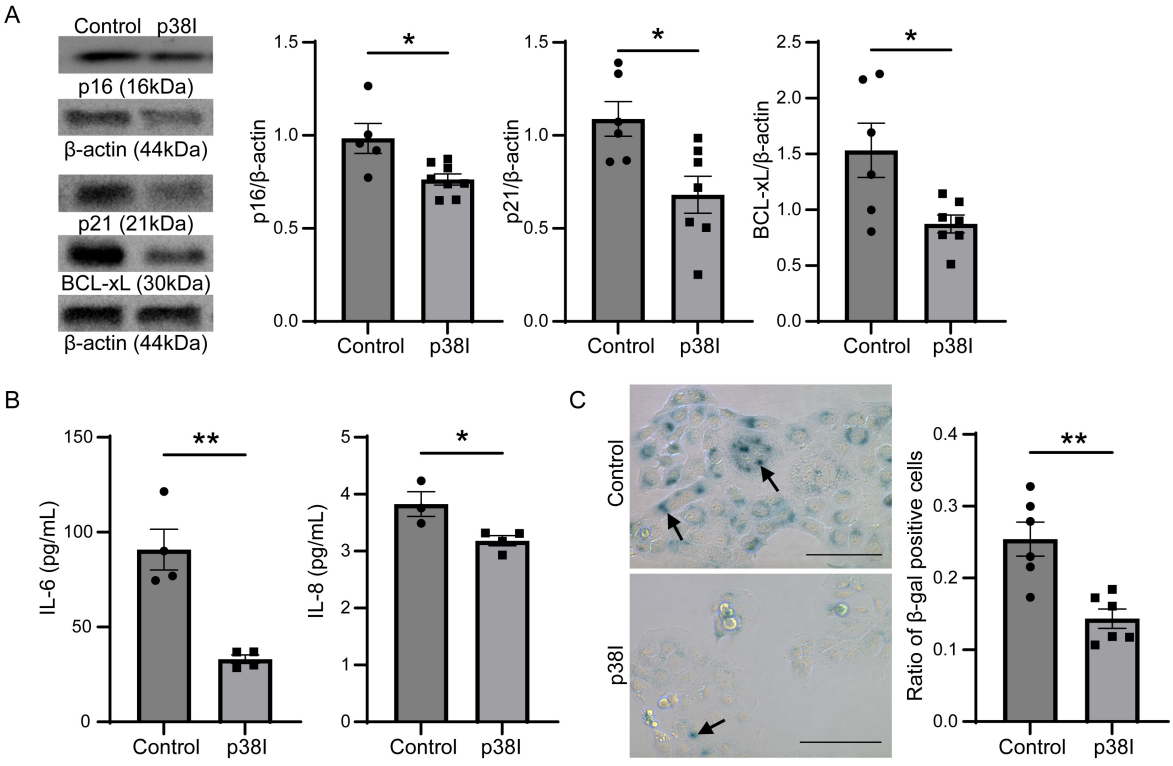

Figure 4: Inhibition of p38 MAPK decreases cellular senescence markers in CFBEs. (A) Representative immunoblot images and densitometric analyses showing p16, p21, and BCL-xL expression of CFBEs treated with SB203580 at 20uM for 24 hours compared to controls (B) Bar graphs showing protein levels of IL-6 and IL-8 in CFBE supernatant after treatment with SB203580 for 24 hours. (C) Representative images of SA- β-gal staining in control and SB203580-treated CFBEs including quantification, arrows indicate β-gal positive cells (scale bar = 100uM, Magnification 40x). Statistical analysis was done using unpaired Student's t-test showing means ± SEM with *$p < 0.05$, **$p < 0.01$, and ***$p < 0.001$ with n =3-5 experiments.

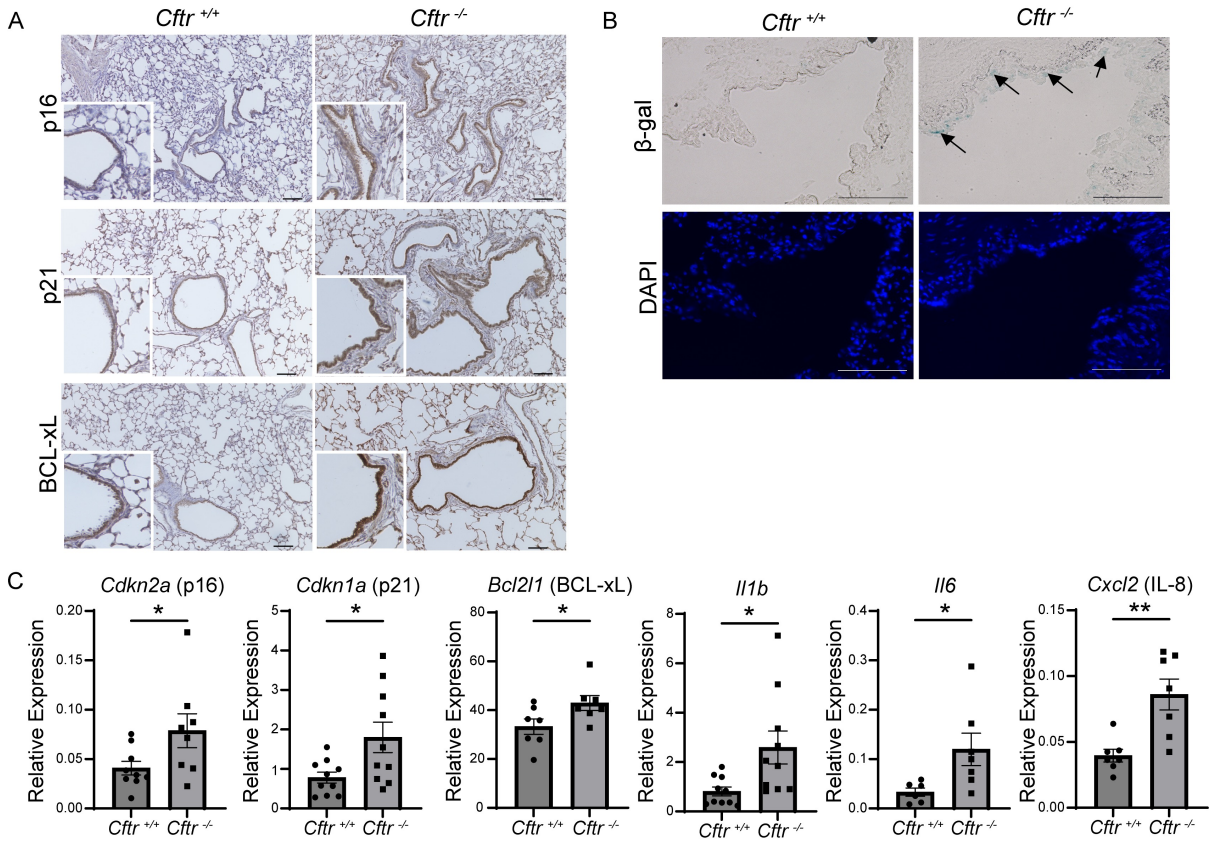

Figure 5: Cellular senescence markers are increased in 6-month-old *Cftr*$^{-/-}$ rat lungs compared to controls. (A) Immunohistochemical staining for p16, p21, and BCL-xL in *Cftr*$^{-/-}$ rat lung tissue compared to controls demonstrating an increased signal in the bronchial epithelium (scale bar= 100uM, magnification 10x). (B) Senescence associated β-gal stain and nuclear counterstain (DAPI) in lung tissue from *Cftr*$^{-/-}$ rats and littermate controls, arrows indicate areas of airway epithelial β-gal staining (scale bar = 100uM, magnification 40x). (C) Relative mRNA levels of *Cdkn2a* (p16), *Cdkn1a* (p21), *Bcl-xL*, and SASPs markers (*Il1b*, *Il6*, and *Cxcl2* (IL-8) normalized to GAPDH, from total lung tissue of control and *Cftr*$^{-/-}$ rats. Statistical analysis was done using unpaired Student's t-test showing means ± SEM with *p < 0.05, **p < 0.01, and ***p < 0.001 with n = 5-10 rats per group and experiments done in triplicates.

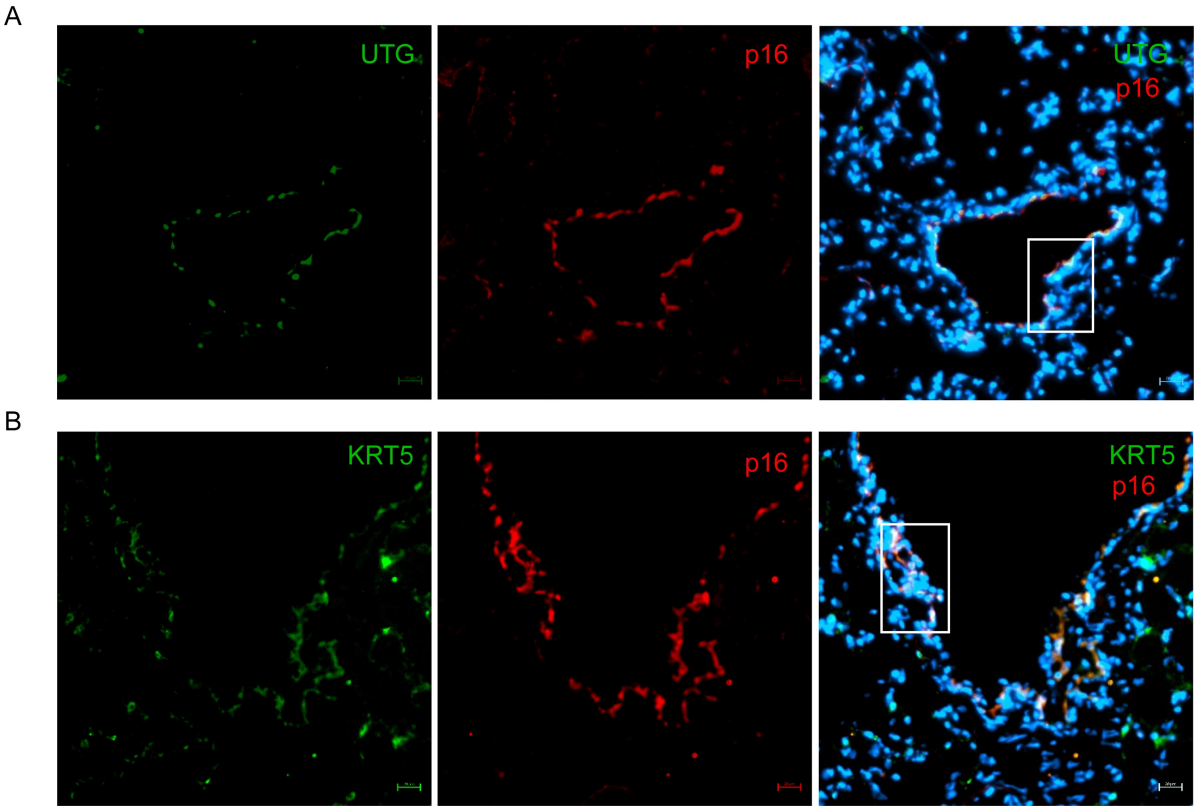

Figure 6: Expression of p16 in both basal cells and secretory airway epithelial cells in 6-month-old *Cftr*$^{-/-}$ rat lungs. A) Immunofluorescence staining for p16 and co-labeled with either Krt5 (KRT5; secretory cells) or Uteroglobin (UTG; basal cells) in *Cftr*$^{-/-}$ rat lung tissue and nuclear staining with DAPI.

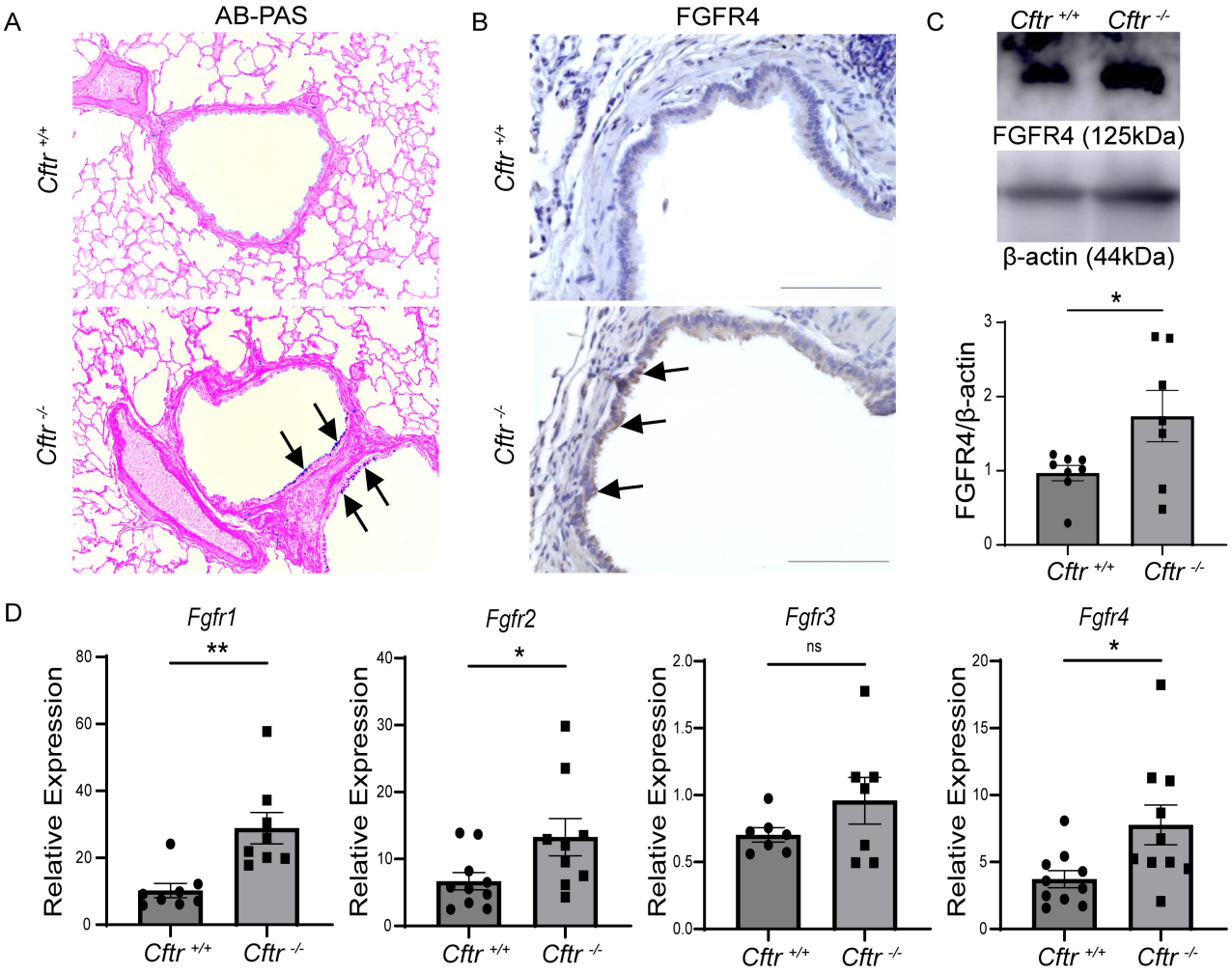

Figure 7: Fibroblast growth factor receptor expression is increased in the lungs of 6-month-old *Cftr*$^{-/-}$ rats.(A) AB-PAS staining indicating an increase of intercellular mucus staining in the bronchial epithelium of *Cftr*$^{-/-}$ rats, compared to control rats, arrows show areas stained in blue for intercellular mucus (magnification 20x) (B) Immunohistochemical analysis using an isoform specific and validated anti-FGFR4 showed increased staining in the bronchial epithelium of *Cftr*$^{-/-}$ rats, arrows highlight areas of airway epithelium stained for FGFR4 (scale bar = 100uM, magnification 40x). (C) Representative images of FGFR4 and β-actin with densitometric analysis demonstrating increased FGFR4 expression in *Cftr*$^{-/-}$ rat airways. (D) Relative mRNA levels of *Fgfr1-4* from *Cftr*$^{-/-}$ total lung tissue, normalized to GAPDH expression. Statistical analysis was done using unpaired Student's t-test showing means ± SEM with *$p < 0.05$, **$p < 0.01$, and ***$p < 0.001$ with n = 5-10 rats per group.

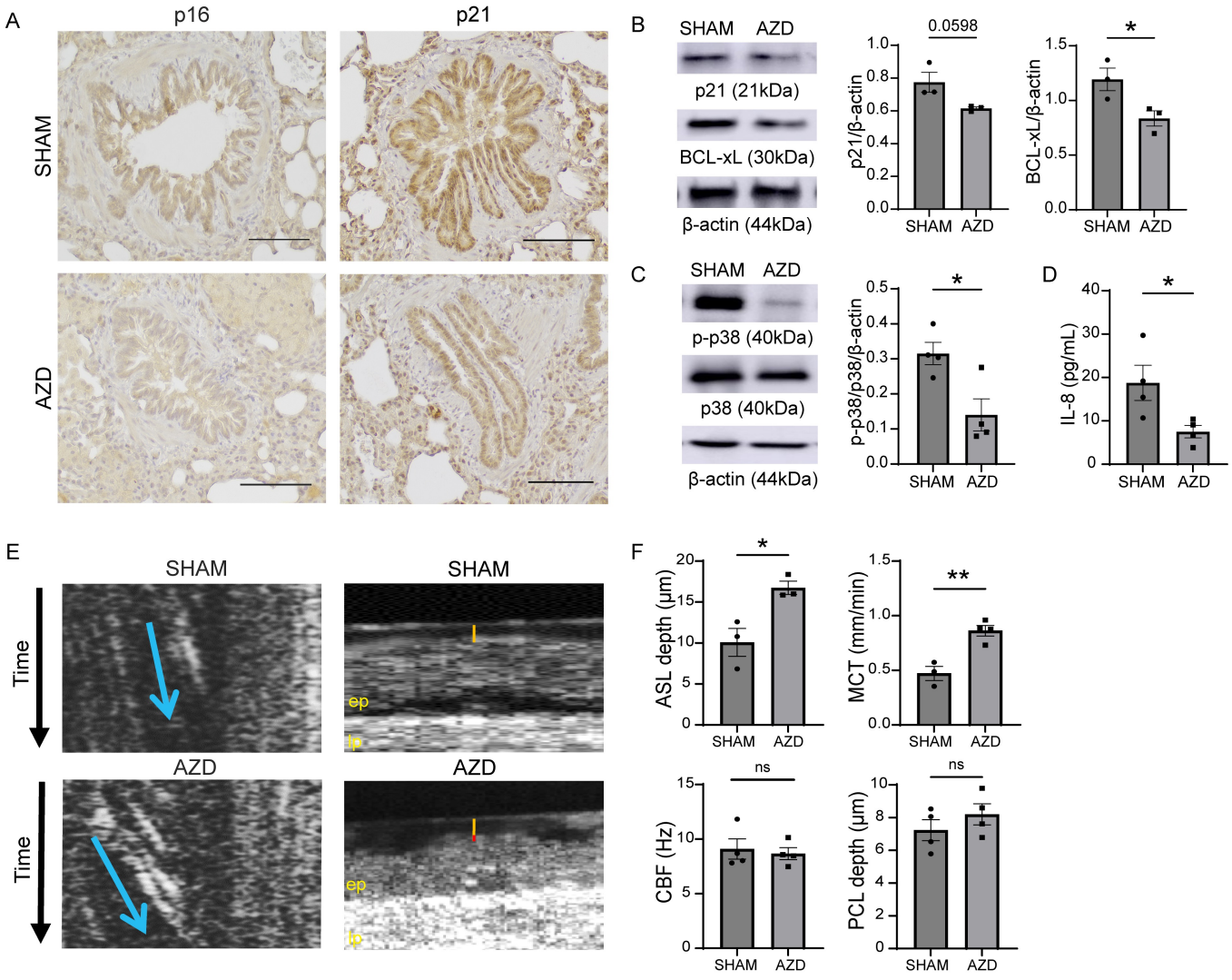

Figure 8: Systemic FGFR inhibition in *Cftr*$^{-/-}$ rats leads to decreased cellular senescence in the lung and improved mucociliary clearance. (A) Representative images of immunohistochemical staining for p16 and p21 in *Cftr*$^{-/-}$ and control rat lungs ± AZD4547 treatment (scale bar = 100uM, magnification 20x). (B) Representative immunoblot images and bar graphs demonstrating densitometric analyses of p21 and BCL-xL protein expression in *Cftr*$^{-/-}$ rat lungs ± AZD4547 treatment. (C) Representative immunoblot images of phosphorylated and total p38 MAPK and densitometric analysis. (D) IL-8 protein levels in *Cftr*$^{-/-}$ rat lung tissue ± AZD4547 treatment. (E) Representative images showing mucociliary transport (MCT) (cross-sectional arrow in blue indicates the velocity of the mucus particle via the slope). Along with, representative uOCT images of the trachea of *Cftr*-/- rats (yellow line representing airway surface liquid depth and the red line representing periciliary liquid depth, ep= epithelial layer, lp= lamina propria). (F) Bar graphs indicating analysis of uOCT images quantifying airway surface liquid [ASL], ciliary beat frequency (CBF), periciliary liquid depth (PCL), and mucociliary transport (MCT) from *Cftr*$^{-/-}$ rat trachea after treatment for 5 days with AZD4547 (12.5 mg/kg) or sham. Statistical analysis was done using unpaired Student's t-test showing means ± SEM with *$p < 0.05$, **$p < 0.01$, and ***$p < 0.001$ with n = 3-4 rats per group.

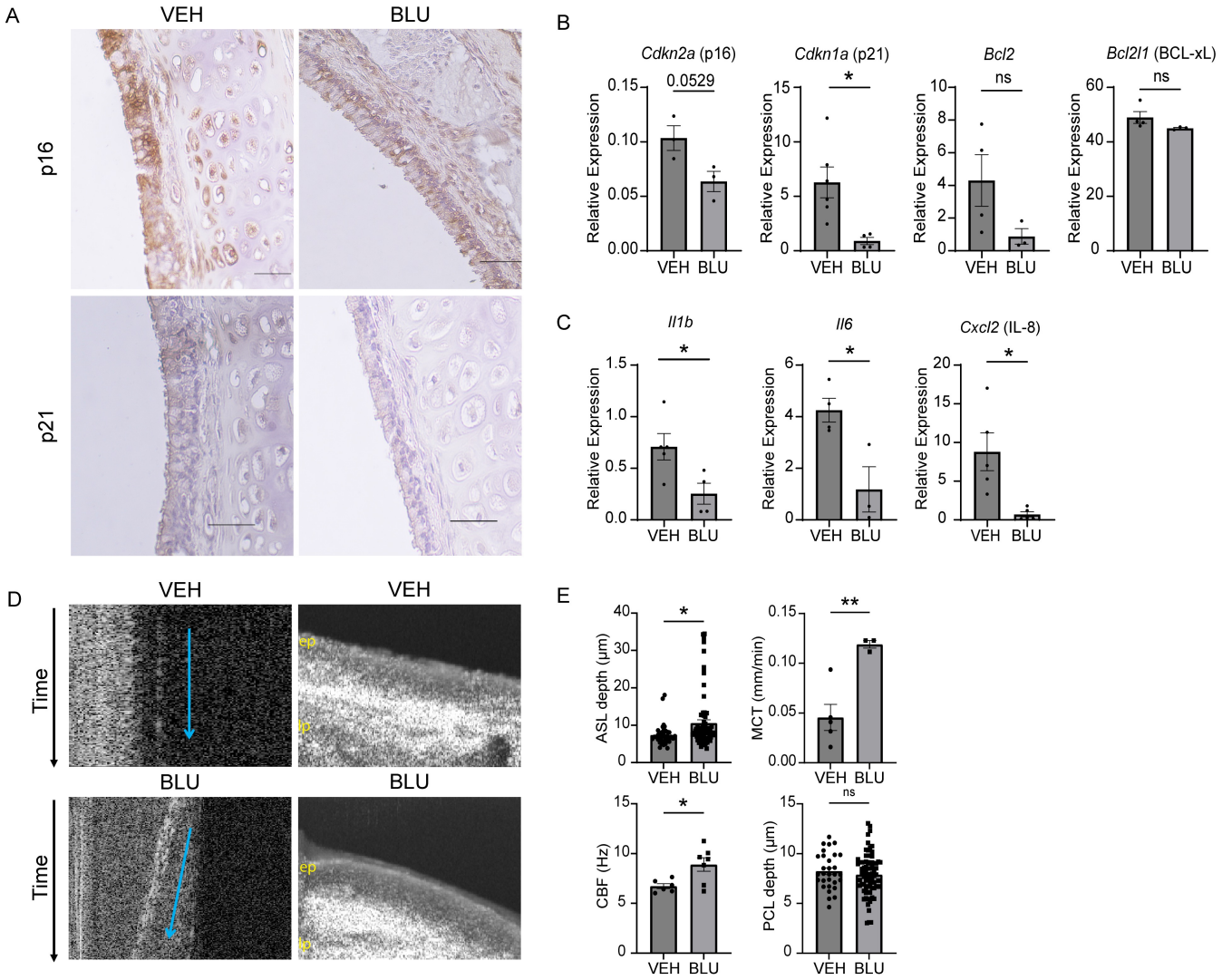

Figure 9: Isoform specific FGFR4 inhibition in an *ex-vivo Cftr*$^{-/-}$ rat trachea model improves mucociliary clearance with attenuation of senescence markers. (A) Immunohistochemistry of p16 and p21 from *ex-vivo Cftr*$^{-/-}$ rat tracheae treated with BLU9931 at 0.1uM for 24 hours compared to vehicle-treated "control" *Cftr*$^{-/-}$ rat tracheae. (B) mRNA levels of *Cdkn2a* (p16), *Cdkn1a* (p21), *Bcl2* and *Bcl2l1* (BCL-xL) and SASP markers (C) *Il1b*, *IL6*, and *Cxcl2* (IL8) from the *ex-vivo Cftr-/-* rat tracheae +/- BLU9931. (D) Representative µOCT images (ep= epithelial layer, lp= lamina propria) and (E) bar graphs showing µOCT quantification of periciliary liquid depth (PCL), mucociliary transport (MCT), ciliary beat frequency (CBF) and airway surface liquid [ASL] depth both from BLU9931 and vehicle control treated *ex-vivo Cftr*$^{-/-}$ rat tracheae. Statistical analysis was done using unpaired Student's t-test showing means ± SEM with *$p < 0.05$, **$p < 0.01$, and ***$p < 0.001$ with n = 3-4 rat trachea per group.

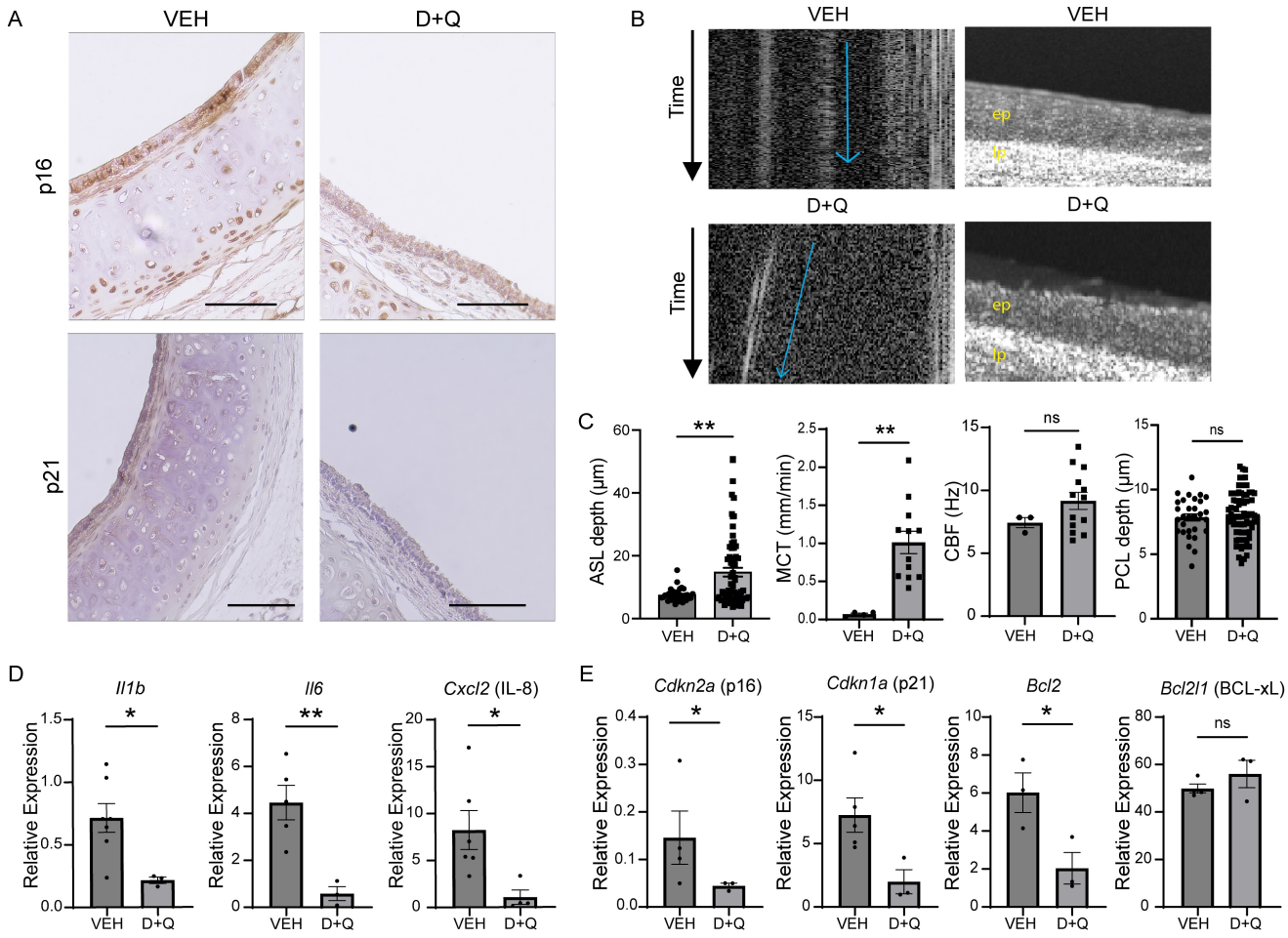

Figure 10: Treatment with Dasatintib and Quercetin (D+Q) significantly decreases cellular senescence and improves mucociliary clearance in the *ex vivo* Cftr$^{-/-}$ rat trachea model. (A) Immunohistochemistry of *Cdkn2a* (p16), *Cdkn1a* (p21) of Cftr$^{-/-}$ rat tracheae, which were treated with 100nM Dasatinib and 2uM Quercetin for 24 hours compared to vehicle treated Cftr-/- rat tracheae. (B) Representative µOCT images of the different Cftr$^{-/-}$ rat trachea groups (ep= epithelial layer, lp= lamina propria) including representative images to assess mucociliary transport (MCT). (C) Bar graphs showing quantification of all regions of interest from µOCT images for assessment of ASL, MCT, CBF and PCL from the vehicle and D+Q treated groups. (D) mRNA levels of SASP markers (*Il1b*, *Il6*, and *Cxcl2* (IL-8)) along with senescence markers *Cdkn2a* (p16), *Cdkn1a* (p21), *Bcl2* and *Bcl2l1* (BCL-xL) from Cftr-/- rat tracheae +/- D+Q. Statistical analysis was done using unpaired Student's t-test showing means ± SEM with *p < 0.05, **p < 0.01, and ***p < 0.001 with n = 3-4 rat tracheae per group.

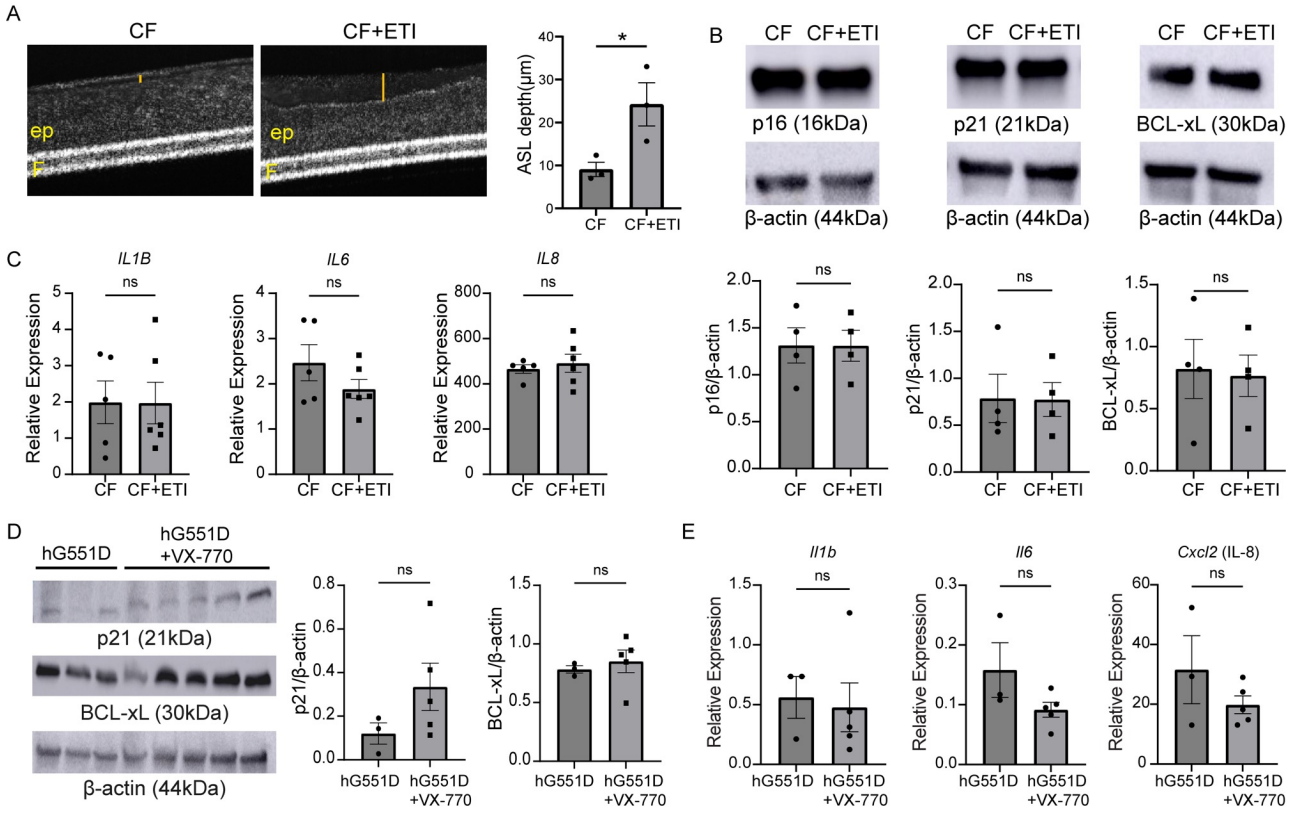

Figure 11: HEMT does not significantly decrease cellular senescence markers or expression of FGFRs. (A) Representative μOCT images and bar graph of CF primary human bronchial epithelial cells (n=3 donors per group) treated with VX-661/VX-445/VX-770 [ETI] for 72 hours showing a significant increase in ASL depth in CF cells treated with ETI, labels: yellow line is ASL depth, ep: epithelial layer and F: filter. (B) Representative immunoblots and densitometric analysis showing no significant difference in protein expression of cellular senescence markers p16, p21 and BCL-xL in CF primary human bronchial epithelial cells treated with ETI for 72 hours when compared to untreated CF primary human bronchial epithelial cells (n= 4 donors per group). (C) Relative expression of SASPs markers (*Il1b*, *Il6*, and *Cxcl2* (IL-8)) from CF primary human bronchial epithelial cells demonstrates no significant change when compared to untreated CF primary human bronchial epithelial cells. (D) Immunoblots and densitometric analysis of p21 and BCL-xL in hG551D rats and hG551D rats treated with VX-770 for 14 days (hG551d= 3 rats, hG551d+VX-770= 5 rats). (E) Relative expression of SASPs markers *Il1b*, *Il6* and *Cxcl2* (IL-8) in hG551D rats and hG551D rats treated with VX-770 for 14 days (hG551d= 3 rats, hG551d+VX-770= 5 rats). Statistical analysis was done using Student's t-test showing means ± SEM with *$p < 0.05$, **$p < 0.01$, and ***$p < 0.001$.